A new method to assess long-term sea-bottom vertical displacement in shallow water using a bottom pressure sensor: application to Campi Flegrei, Southern Italy

Francesco Chierici[1,2,3] , Giovanni Iannaccone[4], Luca Pignagnoli[2], Sergio Guardato[4], Marina Locritani[3], Davide Embriaco[3], Gian Paolo Donnarumma[4], Mel Rodgers[5], Rocco Malservisi[6], Laura Beranzoli[3]

[1] Istituto Nazionale di Astrofisica - Istituto di Radioastronomia, Bologna

[2] Istituto Istituto di Scienze Marine, Bologna

[3] Istituto Nazionale di Geofisica e Vulcanologia, Sezione Roma2, Roma

[4] Istituto Nazionale di Geofisica e Vulcanologia, Sezione di Napoli Osservatorio Vesuviano, Napoli, Italy

[5] University of Oxford, Department of Earth Sciences, Oxford, UK

[6] University of South Florida, School of Geosciences, Tampa, FL, USA

Corresponding authors: Francesco Chierici (chierici@ira.inaf.it) , Giovanni Iannaccone (giovanni.iannaccone@ingv.it)

Index term:

3094 Instruments and Techniques - Marine Geology and Geophysics

8419 Volcano Monitoring - Volcanology

8488 Volcanic Hazards and Risks - Volcanology

key words: Seafloor Geodesy, Submerged Volcanic Areas Monitoring, Bottom Pressure Recorder Measurements, Sea level Measurements

Key Points:

- New method to precisely estimate long term small vertical seafloor displacement along with BPR instrumental drift.
- Geodetic measurements in shallow water environment using BPR and ancillary data.
- Integration of temperature and salinity profiles are essential for BPR interpretation.

Abstract

We present a new methodology using Bottom Pressure Recorder (BPR) measurements in conjunction with sea level, water column and barometric data. to assess the long term vertical seafloor deformation to a few centimeters accuracy in shallow water environments. The method helps to remove the apparent vertical displacement on the order of tens of centimeters caused by the BPR instrumental drift and by sea water density variations. We have applied the method to the data acquired in 2011 by a BPR deployed at 96 m depth in the marine sector of the Campi Flegrei Caldera, during a seafloor uplift episode of a few centimeters amplitude, lasted for several months. The method detected a vertical uplift of the caldera of 2.5 +/- 1.3 cm achieving an unprecedented level of precision in the measurement of the submarine vertical deformation in shallow water. The estimated vertical deformation at the BPR also compares favorably with data acquired by a land based GPS station located at the same distance from the maximum of the modeled deformation field. While BPR measurements are commonly performed in deep waters, where the oceanic noise is relatively low, and in areas with rapid, large-amplitude vertical ground displacement, the proposed method extends the capability of estimating vertical uplifts from BPR time series to shallow waters and to slow deformation processes.

1 Introduction

Magma movement, hydrothermal activity, and changes in pressure in a volcanic system can all result in significant ground deformation (e.g. [Freymueller et al., 2015]). Furthermore, ground deformation is a common precursor to volcanic eruptions [Dvorak and Dzursin, 1997] and the observation of surface deformation is considered one of the primary volcano monitoring techniques (e.g. [Dzursin, 2006]). While continuous surface deformation monitoring is routinely performed on land [Sparks, 2003], monitoring surface deformation of submerged or semi-submerged volcanic fields is more difficult, in particular for shallow water.

Many volcanic fields are at least partially submerged and underwater volcanic edifices can be found in a variety of settings such as at coastal volcanoes, volcanic islands with collapsed and submerged edifices, large caldera lakes, or partially submerged volcanoes in large inland lakes. In addition to typical volcanic hazards, the submerged nature of these volcanoes presents an additional tsunami hazard [Ward and Day, 2001] and the hazard of significant phreatomagmatic eruptions [Houghton and Nairn, 1991; Self, 1983]. Furthermore, many of these volcanoes are close to large cities. Naples (Italy), Kagoshima (Japan), Manila (Philippines), Auckland (New Zealand), Managua (Nicaragua), are examples of cities growing close to the flanks of partially submerged volcanic fields. Many of these volcanic centers have the potential for very large eruptions [Pyle, 1998] often with deep rooted magmatic systems. At these volcanoes, relying on only land-based deformation monitoring restricts the depth at which large magmatic intrusions can be detected and biases modeling of the location of the magmatic source.

Shallow water systems pose a unique challenge for volcano monitoring, as neither traditional land geodesy nor classical deep water marine geodesy are feasible in this 'blind spot'. Extending deformation monitoring to the submerged part of volcanic edifices could significantly improve our ability to understand volcanic processes and therefore improve our monitoring capabilities. Here we present Bottom Pressure Recorder (BPR) data from the Gulf of Pozzuoli collected in 2011 during a small episode of uplift at Campi Flegrei. We demonstrate that by integrating BPR data with local environmental measurements and regional sea level variations from tide gauge network, which provide a guess of the character of the deformation, it is possible to observe seafloor deformation in shallow water (< 100 m) of the order of few centimeters per year. Our results are consistent with the expected deformation from published models of uplift during this same time period constrained by satellite geodesy of the sub-aerial part of the volcanic field [Trasatti et al., 2015].

2 Background

2.1 Recent developments in measuring seafloor vertical displacement

In the last three decades, space geodetic techniques for land deformation monitoring, such as GPS and InSAR, have revolutionized a number of fields in geophysics. Development of seafloor geodesy techniques suitable for the more challenging marine environment has not occurred at the same rate [Bürgmann and Chadwell, 2014]. Seafloor geodesy is primarily based on two methods: a) the measurement of travel time of acoustic wave propagation between fixed points [Spiess et al., 1998; Ikuta et al., 2008], and b) the measurement of hydrostatic pressure at the sea floor [Chadwick et al., 2006; Nooner and Chadwick, 2009; Ballu et al. 2009, Hino et al., 2014].

When the propagation speed of the acoustic wave is known, the distance between a source and receiver can be inferred from the travel time and by combining multiple receivers and sources it is possible to precisely estimate the relative position of a target site [Bürgmann and Chadwell, 2014]. In optimal conditions, such as those found in deep water where salinity and temperature vary little (and thus do not affect significantly the acoustic wave travel times), precisions of 1mm over 1 km baselines have been achieved [McGuire and Collins, 2013]. However, in shallow water large variability of the acoustic wave velocity due to strong lateral temperature variations, significantly limits the application of this technique.

Another common technique in marine geodesy that is suitable for monitoring vertical ground displacement, is based on the variation of hydrostatic pressure at the sea bottom. Although the water density depends on the time variability of temperature and salinity, in case where this variation is not significant or is known, the variation of the pressure can be related to changes in the height of the water column. Consequently, a sea bottom monitoring system for continuous measurement of water pressure can be used to estimate the vertical movement of the seafloor.

Currently, the most common technology to measure pressure at the sea floor uses a Bourdon tube: the extension or shortening of the tube due to changes of pressure is measured by a quartz strain gauge via the frequency variations of the quartz oscillator [Eble and Gonzales, 1991]. Bottom Pressure Recorders (BPR) using a Bourdon tube can provide a resolution corresponding to variations of a few millimeters over a water column of 6000 meters. This kind of sensor is very commonly used in the measurement of short term transient signals like the variation of pressure due to the passage of a tsunami wave. For example, the tsunami alert system DART (Deep-ocean Assessment and Reporting of Tsunamis) used by the US National Oceanic and Atmospheric Administration (NOAA) includes oceanographic buoys acoustically connected to sea floor stations equipped with a Bourdon tube technology BPRs [Bernard and Meinig, 2011].

From the 1990s this technology has also been used to measure tectonic deformation [Fox, 1990; 1993; 1999; Fox et al., 2001; Hino et al., 2014; Wallace et al., 2016], and to study the dynamics of deep water submerged volcanic areas [Phillips et al., 2008; Ballu et al., 2009; Chadwick et al., 2006; Nooner and Chadwick, 2009; Chadwick et al., 2012; Dziak et al., 2012]. The majority of the published papers using BPRs for measurement of vertical displacement of the sea floor refer to depths larger than 1000 m, where the effect from waves is minimal. On the other hand, near surface processes are much stronger for measurements carried out in water less than 200 - 300 m depth, producing noisy records that are very difficult to interpret.

One of the largest limitations in the use of quartz technology for BPRs is the drift. These instruments tend to have sensor drift of up to tens of cm/yr, with amplitude and polarity that are not predictable and are different for each sensor [Polster et al., 2009]. Laboratory experiments by Wearn and Larson [1982] at a pressure of 152 dbar (corresponding to a depth of approximately 150 m) show that quartz technology BPR drift is several mbar during the first 100 days. The variation is larger (following an exponential behavior) during the first 20 days after the deployment then the drift is approximately linear thereafter [Watts and Kontoyiannis, 1990]. It was also observed that operating the instrument in shallow water can reduce the drift amount [Wearn and Larson, 1982].

Such high amounts of drift could potentially mask any tectonic or volcanic signals [Polster et al., 2009]. An active area of research is the design of non-drifting sensors (e.g. [Gennerich and Villinger, 2015]), the development of self-calibrating instruments (e.g. [Sasagawa and Zumberge, 2013]) and the methodologies to correct the measurements for drift, as for instance the ROV-based campaign-style repeated pressure measurements at seafloor benchmarks outlined in Nooner and Chadwick (2009).

2.2 Summary of Campi Flegrei activity

Campi Flegrei (Figure 1) is a volcanic caldera located west of Naples in the South of Italy that is continuously monitored by the Italian National Institute of Geophysics and Volcanology (INGV, http://www.ov.ingv.it/ov/en/campi-flegrei.html). The complex contains numerous phreatic tuff rings and pyroclastic cones and has been active for the past 39,000 years [Di Vito et al. 1999]. This area is known for repeated cycles of significant slow uplift followed by subsidence [Del Gaudio et al., 2010]. Although long-term changes in deformation do not necessarily culminate in eruption, the most recent eruption in 1538 was preceded by rapid uplift, demonstrating the importance of surface deformation as a monitoring tool [Di Vito et al., 1987]. Since 1969 the caldera has had significant episodes of uplift with more than 3 m of cumulative uplift measured in the city of Pozzuoli in the period 1970-1984 [Del Gaudio et al., 2010]. After 1984 the area subsided but was interrupted by small episodes with uplift on the order of a few cm [Del Gaudio et al., 2010; De Martino et al., 2014b]. The subsidence phase stopped in 2005 when a new general uplift phase began. At the time of submission of this paper the uplift has reached a cumulative vertical displacement of about 36 cm. In 2011 Campi Flegrei was subject to an acceleration of the uplift trend that was recorded by the on-land geodetic network with a maximum value of approximately 4 cm, as measured at Pozzuoli GPS station over the whole year [De Martino et al., 2014b]. However, the center of the caldera (and presumably the area of maximum uplift) is located off-shore.

2.3 Instrumentation and Data

The Campi Flegrei volcanic area is monitored by multiple networks that are all centrally controlled by the Neapolitan branch of INGV (Figure 1). The land based monitoring system consists of 14 seismic stations, a geodetic network of 14 continuously operated GPS (CGPS) and 9 tilt-meters. The Gulf of Pozzuoli represents the submerged part of the caldera and marine monitoring within and around the Gulf consists of 4 tide gauges and a marine multiparametric system (CUMAS), described below. INGV are also developing new marine monitoring techniques, such as underwater monitoring modules and geodetic buoys [Iannaccone et al, 2009; 2010; De Martino et al. 2014a].

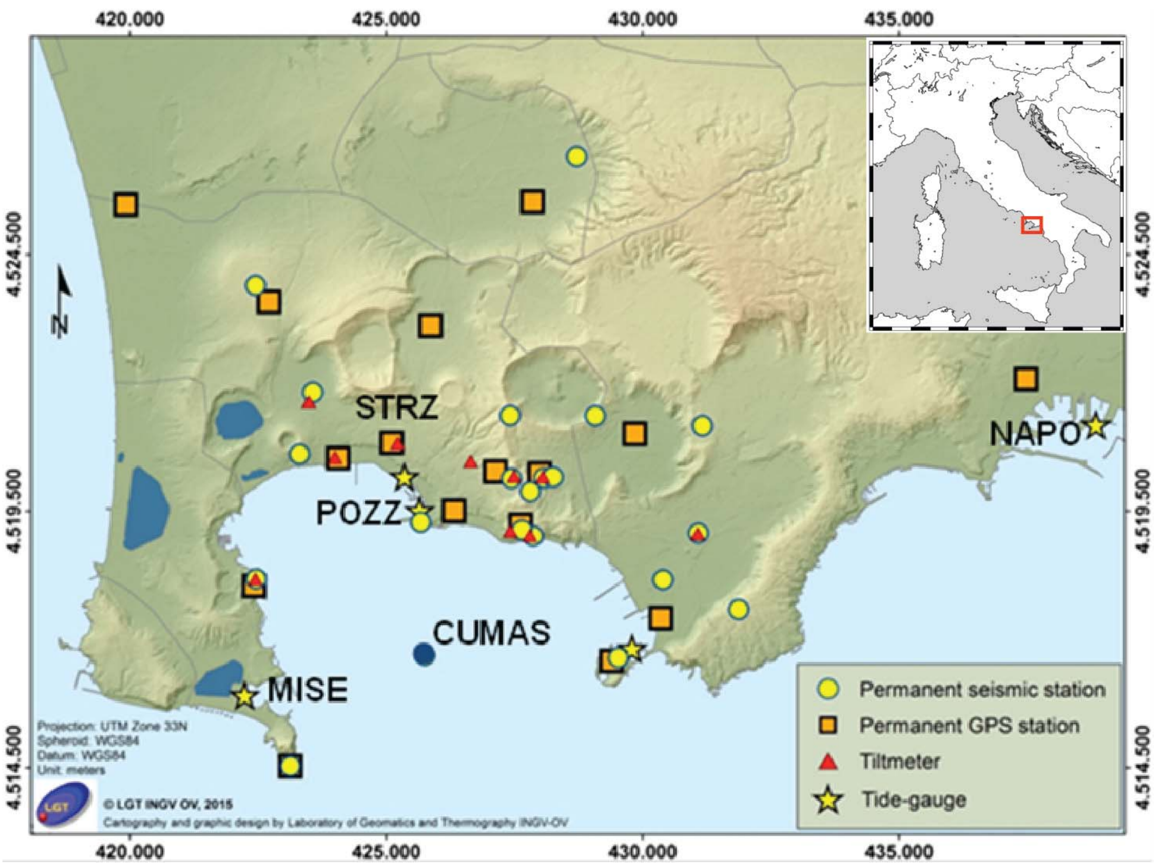

Figure 1. Map of the geophysical permanent monitoring network of Campi Flegrei. Yellow dots = seismic stations; orange squares = permanent GPS stations; red triangles = tilt-meters; yellow stars = tide-gauges. Blue dot represents the location of CUMAS multi-parametric station and of the BPR used in this work.

The longest time series that can be used for marine geodetic studies in this area comes from the network of tide gauges, and these have monitored all the deformation episodes over the last 50 years [Berrino, 1998; Del Gaudio, et al., 2010]. Tide gauges provide a continuous time series of sea level at a given location. If the elevation of the tide gauge changes, the instruments record this as a relative change in sea level. Therefore it is necessary to distinguish between sea level changes and vertical movements of the gauge. This can be done by deconvolving the observed data with measurements from nearby reference stations located outside the deforming region (e.g. [Berrino, 1998]), or via subtraction of the moving average of data from the reference station [Tammaro et al., 2014]. This kind of analysis is typical for monitoring of active volcanic areas (e.g. [Corrado and Luongo, 1981; Mori et al., 1986; Paradissis et al., 2015]). The tide gauge station NAPO (Figure 1) is located within Naples' harbor, and repeated precise leveling and GPS campaigns have shown this station to be outside the Campi Flegrei deformation area [Berrino, 1998]. Hence in this work we use this station as a reference station.

Within the Gulf of Pozzuoli a permanent marine multi-parametric station (named CUMAS) has been operating intermittently since 2008 [Iannaccone et al., 2009; 2010]. This station is a marine infrastructure elastic beacon buoy, equipped with various geophysical and environmental sensors installed both on the buoy and in a submerged module lying on the seafloor (~ 96 m deep). Among the instruments installed in the underwater module, there is a broadband seismometer, a hydrophone, and a quartz technology Paroscientific series 8000 BPR. Unfortunately, due to biological fouling and corrosion of the sensor components arising from incorrect coupling of different types of metals on the same sensor, the availability of the BPR data is limited to a short period during 2008 and about seven months during 2011.

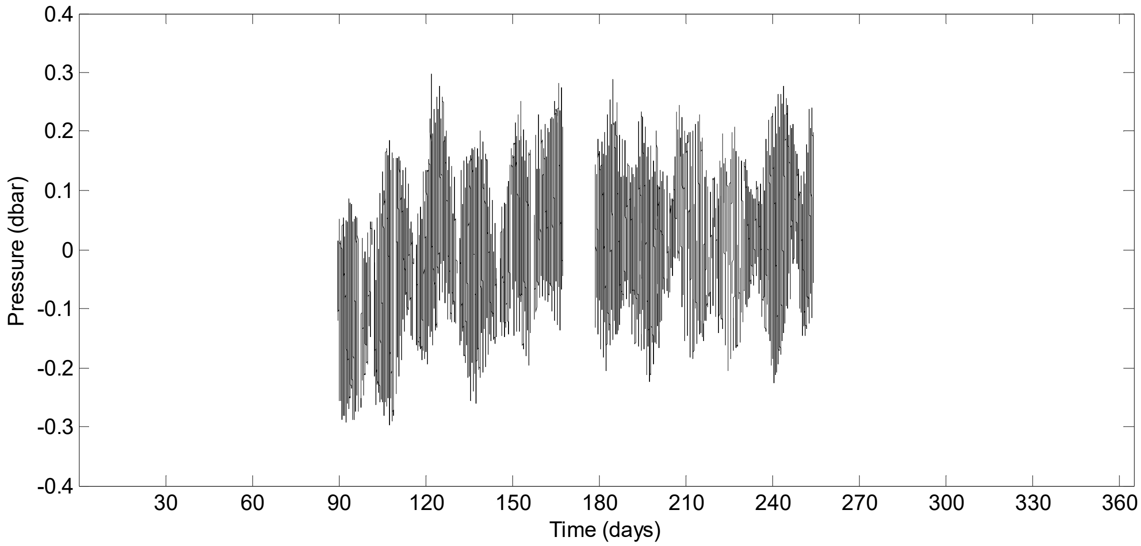

Figure 2. Bottom pressure time series acquired by the BPR deployed at CUMAS site (96 m depth) from the end of March to September 2011

The raw data during the 2011 BPR deployment are shown in Figure 2. The BPR time series contains some gaps due to interruption in the data flow from the CUMAS buoy to the land station, the largest one is ~12 days during the month of June.

3 Methods: Signal components and correction methods

As stated by Gennerich and Villinger [2011], it is very difficult to separate the component of variation of sea bottom pressure due to oceanographic and meteorological origin from the tectonic signals we are interested in. In this paper we attempt to distinguish vertical displacement of the seafloor by estimating the variation of the water column height above the BPR sensor. We combine this with both sea level data acquired from tide gauges located in the nearby region, and with local environmental data (salinity, temperature, air pressure).

It is important to stress that tide gauges and BPRs measure different physical quantities: tide gauges measure time variation of the sea level while BPR measures time variation of the pressure at the sea floor. To obtain seafloor deformation from these two observations it is necessary to clean the two time series from the effects of other phenomena that could affect the measurements (e.g. tide, atmospheric pressure, salinity and temperature), and to convert them to the same physical observation (vertical displacement of the sensor).

The sea level L(t) measured by the tide gauge can be described by the following equation:

$$L(t) = L_0 + \Delta L(t) + \frac{\Delta P_{atm}(t)}{\rho(t,T,S)g} + h_{TG}(t) \qquad (1)$$

where L_0 represents the average sea level (considered constant during the time of our measurements, i.e. not taking into account long term phenomena like sea level rise due global warming etc.) $\Delta L(t)$ includes oceans waves, astronomical (e.g. tides), and oceanographic components (e.g. tidal resonances and seiches); the term $\Delta P_{atm}(t)/\rho(t,T,S)g$ describes the effect of the variation of atmospheric pressure (known as inverse barometric effect, [Wunsch and Stammer, 1997]). In this term ρ is the sea water density depending on the temperature T and salinity S and g is the acceleration of gravity; $h_{TG}(t)$ describes the apparent sea level change due to the vertical deformation of the area (i.e. of the vertical displacement of the sensor). By measuring L(t) and correcting for the first 3 terms of the right side of equation (1) it is possible to derive $h_{TG}(t)$.

Similarly to the tide gauge data, the seafloor pressure data derives from superposition of different components. The observed pressure can be described by the combination of the hydrostatic load (which is dependent on the height of the column of water), and the effect due to average density of the water column caused by variation of temperature, pressure, and salinity. The changes of pressure at the seafloor $P_{bot(t)}$ can be described by

$$P_{bot}(t) = \rho_0 g \bar{H} + \rho_s \Delta H(t) g + \rho_b h_b(t) g + g \int_{-H}^{0} \Delta\rho(t, T, S, P)\, dz \qquad (2)$$

In this equation the term $\rho_0 g \bar{H}$ represents the hydrostatic load due to the average height of the water column $\bar{H}$, including the atmospheric pressure; $\rho_s \Delta H(t) g$ is the astronomical and oceanographical component (e.g. tide, waves, seiches); $\rho_b h_b(t) g$ represents the vertical displacement of the seafloor due to the deformation.For each of these terms it is necessary to consider the correct value of the seawater density ρ. In equation (2), ρ_0 represents the average density of the water column and ρ_s and ρ_b are the surface and the bottom densities of the water in the study area. In the last term in the second member of equation 2 of equation (2) Δρ represents the variation in time of the sea water density along the water column. As in equation

(1) T and S represent the temperature and the salinity and P is the water column pressure. Finally, g represents the gravitational acceleration. If all the components in equation (2) are known then the BPR data can be converted to vertical displacement of the seafloor $h_b(t)$ and compared with $h_{TG}(t)$.

As mentioned above, BPR measurements are affected by instrumental drift, which can vary considerably from sensor to sensor and from campaign to campaign [Chadwick et al., 2006; Polster et al., 2009]. Despite these variations the general functional form of the drift can be described by the following equation [Watts and Kontoyiannis, 1990]:

$$D_{BPR}(t) = a\, e^{-bt} + c\, t + d \qquad (3)$$

in which the four parameters a, b, c, d are dependent on the characteristics of each sensor and deployment.

The noise associated with BPR measurements can be described as:

$$R_{BPR}(t) = E_{BPR}(t) + D_{BPR}(t) + O_P(t) \qquad (4)$$

where $E_{BPR}(t)$ is the pressure fluctuation due to instrumental noise, $D_{BPR}(t)$ the instrument drift, and $O_P(t)$ the environmental noise.

Similarly, the tide gauge noise can be described by

$$R_{TG}(t) = E_{TG}(t) + O_{TG}(t) \qquad (5)$$

where $E_{TG}(t)$ is the instrumental noise and $O_{TG}(t)$ is the environmental noise.

4 Data Analysis

During 2011 the GPS network and satellite interferometry detected an uplift episode in the Campi Flegrei area, observed also by the tide gauges POZZ and MISE located in the Gulf of Pozzuoli. Modeling of the source of deformation suggests that it is related to a possible dyke intrusion close to the centre of the caldera [Amoruso et al., 2014b; Trasatti et al., 2015]. Usually during uplift events POZZ registers the largest deformation values, indicating its proximity to the source of the 2011 uplift [De Martino et al. 2014b; Amoruso et al., 2014]. The value of vertical deformation decreases monotonically away from the harbor area of Pozzuoli (station POZZ) reaching a minimum at the MISE station located at the edge of the caldera [De Martino et al., 2014b]. The CUMAS multi-parameter station is deployed approximately halfway between the sites of POZZ and MISE, thus we would expect to observe vertical uplift with values in-between those observed at the two tide gauges.

Following equations (1) and (2), to obtain $h_{TG}(t)$ and $h_b(t)$, which represent the vertical displacement measured by tide gauge and BPR respectively, we need to remove the tidal and meteorological contributions from the tide gauge data, and the tidal and the sea water density variation for the BPR data. Then the vertical sea floor deformation is obtained by subtracting the reference time series of the NAPO tide gauge from the BPR measurement. In the case of sea level data acquired by multiple nearby tide gauges, many terms of equation (1) can be considered to be the same at all the stations. This significantly simplifies the problem since after subtracting the reference sea level the only surviving term is the vertical displacement $h_{TG}(t)$ at the displaced station; this term can be assumed equal to zero at the reference station of NAPO.

4.1 Tide gauge data analysis

The time series acquired by the tide gauges of NAPO, POZZ and MISE in 2011 are shown in Figure 3a,b,c. Assuming that the first three terms in the second member of equation (1) are the same for the stations NAPO, POZZ, and MISE, as mentioned before, it is quite simple to recover possible vertical deformation signals of MISE and POZZ with respect to NAPO by subtracting the raw data of the two stations located in the active volcanic area from the raw data acquired by the reference station NAPO [Tammaro et al., 2014].

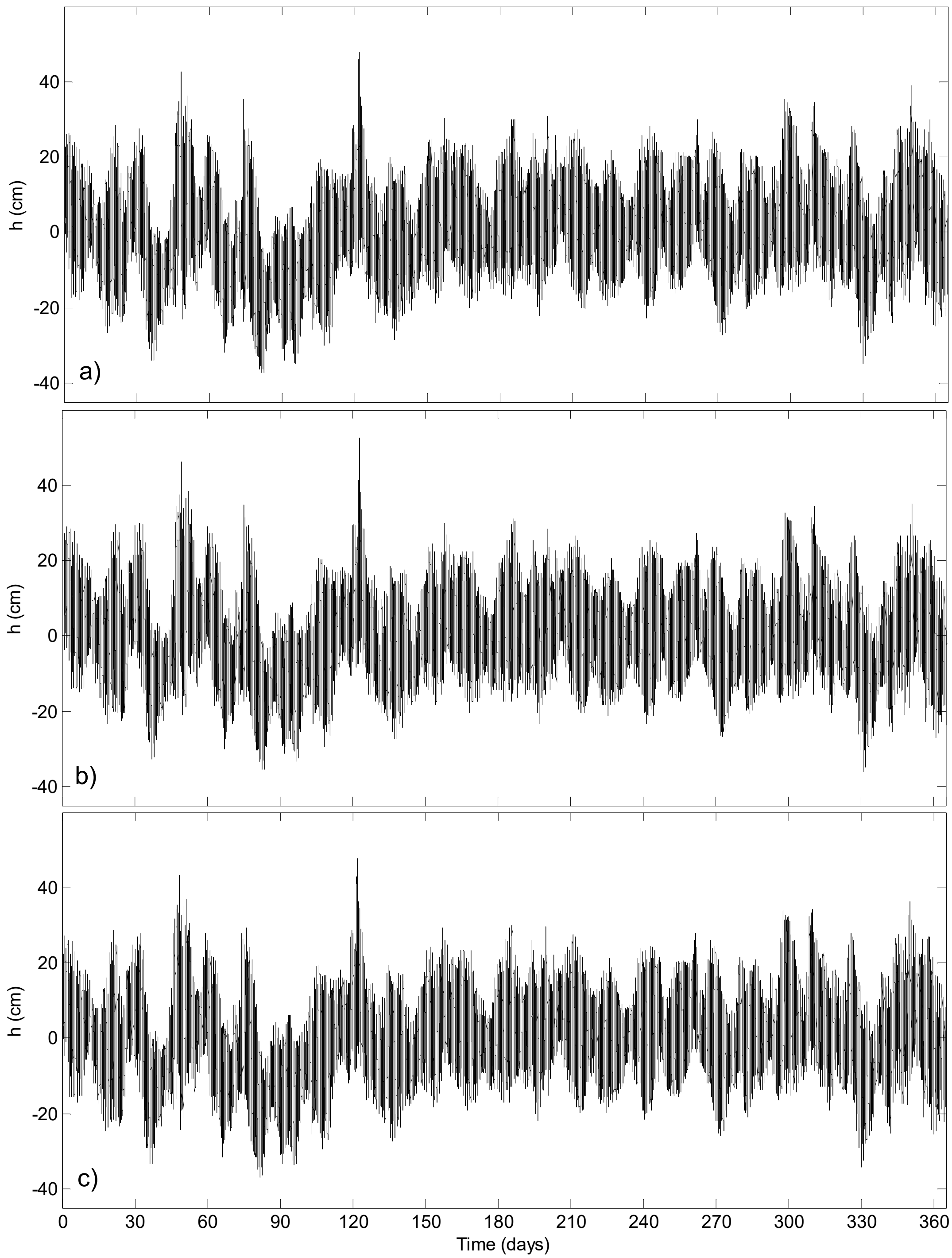

Figure 3. Sea level time series acquired in 2011 by **a**) Napoli tide gauge (NAPO), **b**) Pozzuoli (POZZ) and **c**) Capo Miseno (MISE).

We have averaged the 2011 time series from NAPO, MISE, and POZZ by considering the mean value of contiguous 48-hour time windows and calculating the differences NAPO-POZZ and

NAPO-MISE (Figure 4). These differences represent the term $h_{TG}(t)$ of equation (1) for sites POZZ and MISE with respect to NAPO (from here on termed $h_{TG\_POZZ}(t)$ and $h_{TG\_MISE}(t)$).

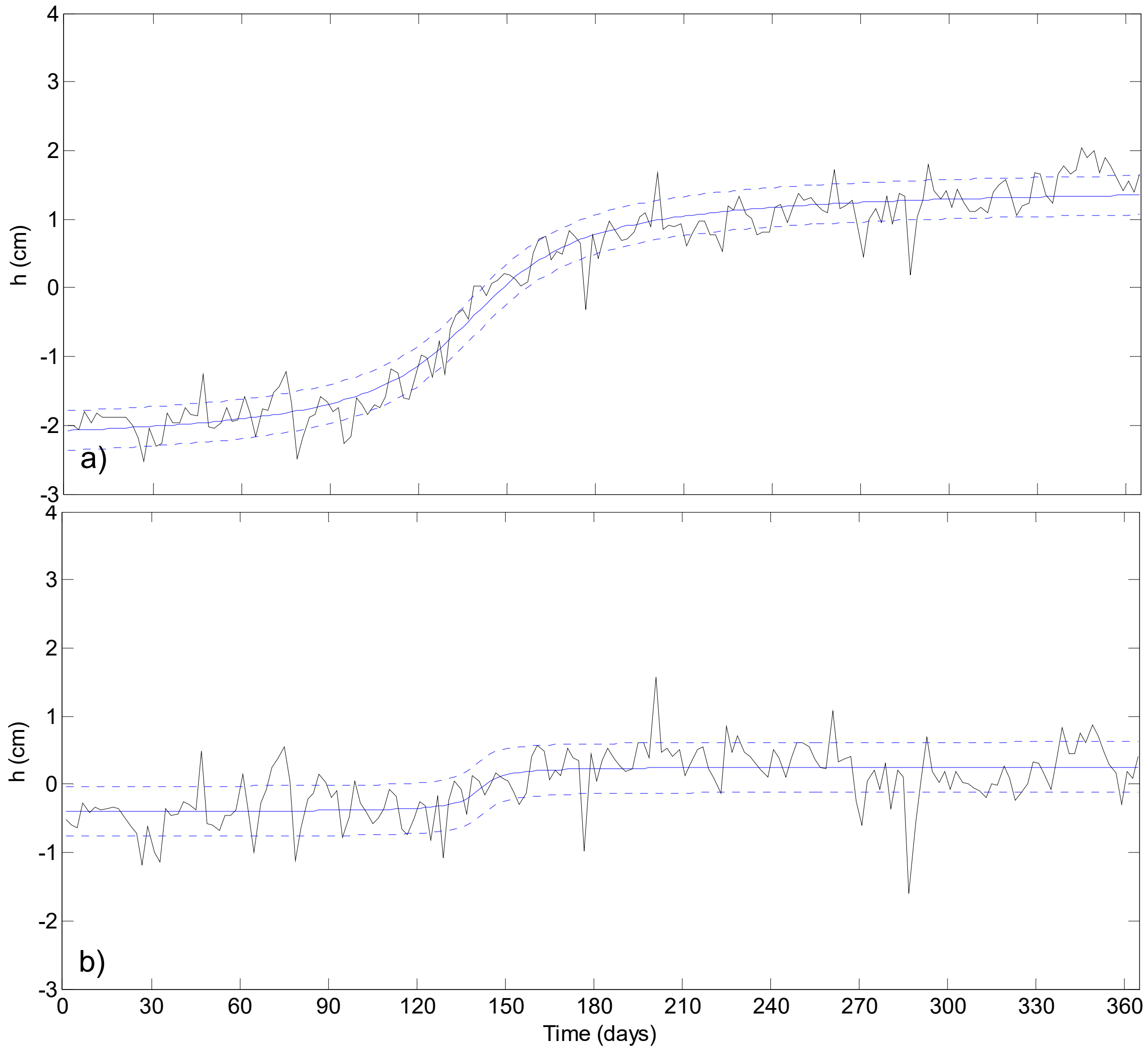

Figure 4. Time series NAPO-POZZ and NAPO-MISE (black solid line), with superimposed (blue solid line) the best fitting vertical deformation $h_{TG\_POZZ}(t)$ at POZZ tide gauge station (panel **a**) and $h_{TG\_MISE}(t)$ at MISE tide gauge station **(**panel **b**). The dashed blue line correspond to 95% confidence intervals for the best fitted data.

The best fits of NAPO-POZZ and NAPO-MISE can be regarded as representative of the vertical deformation at POZZ and MISE locations. After trying various functional forms we decided that the uplift event can be easily and accurately represented by an arctangent function $f(t) = \alpha \tan^{-1}(\beta t + \varphi) + \delta$ (6) where α, β, φ and δ are the coefficients obtained by least square best fitting. Figure 4 shows the arctangent best fitting function and confidence interval for the observed $h_{TG\_MISE}(t)$ and $h_{TG\_POZZ}(t)$. The observed values of the vertical deformation at POZZ and MISE sites during the 2011 period are 3.2 ±0.5 cm and 0.8 ±0.6 cm respectively. We use the arctangent functional form because it minimizes the number of free parameters used in the fit and the rms value of the difference between the data and the model with respect to polynomial fits (see Figure 5).

.

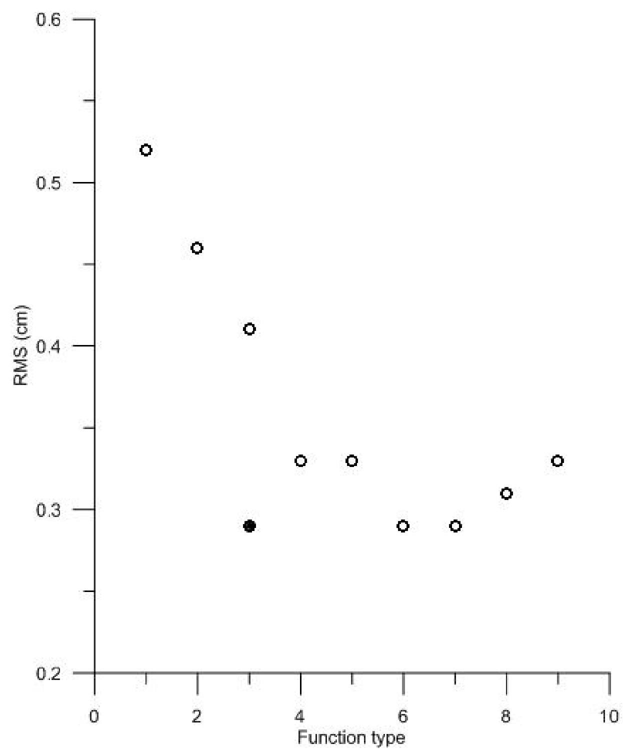

Figure 5. Plot of RMS values of the difference between the NAPO-POZZ time series and the fitting models (polynomial and arctangent) vs the polynomial degree. On the horizontal axis, labeled as function type, is the polynomial degree. The full circle represents the arctangent function described by equation (6), which is characterized by 4 free parameters and hence is plotted at the same abscissa of a degree 3 polynomial.

Unlike the simplicity of the comparison between tide gauge data sets, the comparison between tide gauge and BPR time series requires additional work. This consists of the removal of tidal components and effects of atmospheric pressure described in equation (1) from the tide gauge time series. The tides are removed by computing the specific harmonic frequencies related to the astronomical parameters using the method of Hamels [Pawlowicz et al., 2002], based on a least squares harmonic fitting method. The coefficients of the first 37 tidal components are derived using the T_Tide software described by Pawlowicz et al. [2002]. The time series for NAPO with the tidal signal removed is shown in Figure 6a (black line). After the tidal corrections, the time series are still strongly affected by atmospheric pressure loads as indicated by the strong correlation with the observed atmospheric pressure (red line, scaled in equivalent water height).

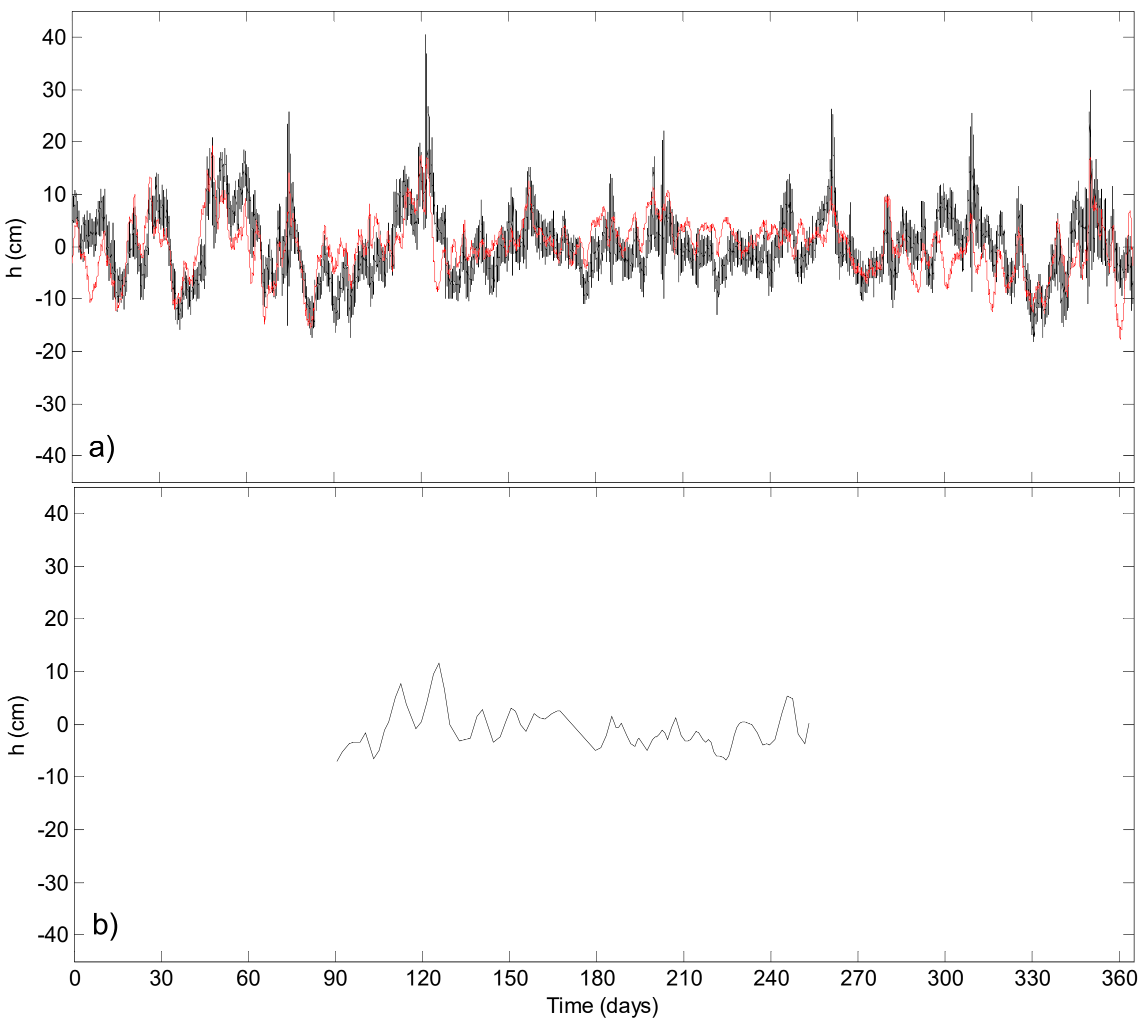

Figure 6. a) NAPO station time series, black line, cleaned by removing the astronomical tide component up to order 37. The red line corresponds to the inverse of the atmospheric pressure at

the NAPO location expressed in equivalent water height. Note the high correlation between the observed value at the tide gauge and the atmospheric pressure multiplied by -1; **b**) NAPO tide gauge observation for the period when the BPR data are available cleaned by subtracting the effect of tide and atmospheric pressure which is used as reference sea level.

Following Wunsch and Stammer [1997], and as described in equation (1), the sea level signal still needs to be corrected for variations due to atmospheric pressure using the average bulk density of the water column (1028 kg/m^3) derived by CTD measurements for the Gulf of Pozzuoli provided by the marine biology institute "Stazione Zoologica Anton Dohrn" of Naples (hereinafter referred to as SZN). The corrected NAPO time series, cleaned of both astronomical tides and atmospheric pressure effects for the period when BPR data are available, is shown in Figure 6b. In this corrected time series oceanographic signals such as regional and local seiches, and waves, are still present. Prior work has shown that for the Gulfs of Naples and Pozzuoli the characteristic eigen-periods of the seiches are shorter than 60 minutes [Caloi and Marcelli, 1949; Tammaro et al., 2014], and that for the full Tyrrenian basin the fundamental seiche eigen-period is 5.70 hours [Speich and Mosetti, 1988]. Since these contributions have periods that are much shorter than the characteristic time of the deformation episode we are interested in, we will consider these signals as part of the high frequency noise in the tide gauge time series. As mentioned before we use the corrected NAPO time series in figure 6b as the sea level reference for the analysis of the BPR data.

4.2 BPR data analysis

The BPR measures time variation of the pressure at the sea floor while tide gauges measure time variation of the sea level. To obtain seafloor displacement using these two observables we need to convert them to the same physical quantity by taking into account tide, atmospheric pressure, and seawater density variation, as described in equations (1) and (2). The tidal component of the BPR data is computed in the same way as for the tide gauge using T_Tide software with up to 37 harmonic components. The water density variation is computed through an integration along the water column of the term $\Delta\rho$ of equation 2 using the sea water equation EOS80 [Fofonoff and Millard 1983] and the CTD profiles from SZN (16 CTD casts, about 1 per month, during 2011). The EOS80 model gives the value for sea water density ρ at a given salinity and temperature. In figure 7 the temperature and salinity profiles used are shown.

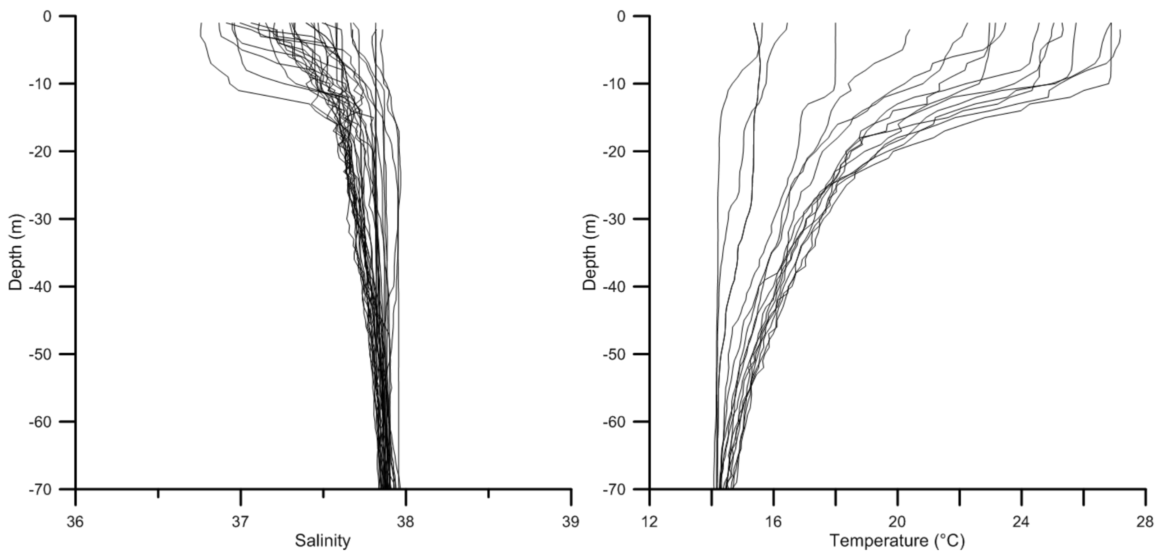

Figure 7. Salinity and temperature profiles measured by SZN during the year 2011 in the Gulf of Naples

The EOS80 equation also accounts for the variation of water density due to hydrostatic contribution. In our case this effect is negligible given the shallow water environment, i.e. at 96 m of water depth, the effect amounts only to about 1 mm of equivalent water height (Fofonoff and Millard 1983). Taking into account tides and water density variation in equation (2) and converting them to equivalent seawater height, we calculate the variation of sea level at the location of the BPR station. By comparing this quantity with the sea level reference (Figure 6b) we obtain a residual time series containing three effects: the vertical displacement of the sea floor at the location of CUMAS multi-parametric station, the BPR instrumental drift, and environmental noise (Figure 8a).

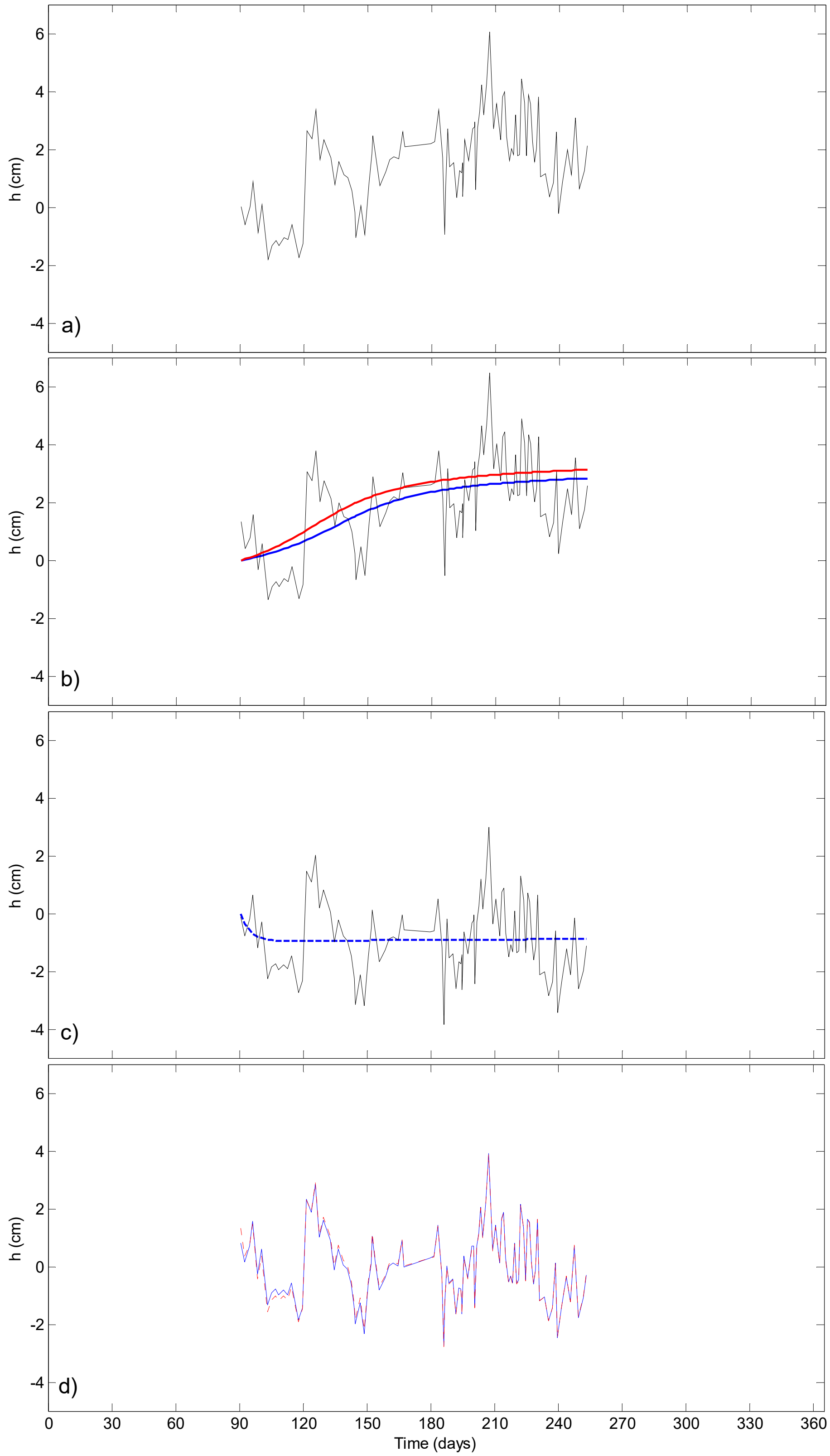

a)
b)
c)
d)
h (cm)
6
4
2
0
-2
-4
0
30
60
90
120
150
180
210
240
270
300
330
360
Time (days)

Figure 8.a) Difference between the sea level measured at the tide gauge NAPO and the sea level calculated from the pressure measured at the BPR. The data in the graph include vertical seafloor deformation observed at the BPR, instrument drift , and environmental noise; **b**) 2011 sea floor uplift at CUMAS site estimated by performing a best fit (blue curve). In red is the same best fit before the correction for the estimated BPR instrumental drift; **c**) Estimated BPR instrumental drift plotted in blue superimposed on the residual time series corrected for the vertical deformation trend; **d**) Comparison between residual time series obtained by subtracting the estimated contribution of the seafloor deformation and of the instrumental drift from NAPO-BPR time series after 1 and n recursions (see text for explanation).

To evaluate these two contributions we use an approach consisting of best fitting the deformation of the sea bottom and then the instrumental drift. Since we assume that the seafloor deformation at the CUMAS site is caused by the same deformation event which uplifted the POZZ and MISE tide gauge sites, we choose to fit the residual time series using the same arctangent function used to fit the time series $h_{TG\_POZZ}(t)$ and $h_{TG\_MISE}(t)$ (Figure a,b). After subtracting the best fit arctangent of the residual time series we estimate the instrumental drift by performing a best fit procedure using the functional form given by equation (3). We then use the obtained drift to estimate the true sea bottom displacement using a recursive procedure. This is accomplished by subtracting the obtained drift from the residual time series and then re-computing the coefficient of the arctangent best fit to recover the true sea bottom displacement (Figure 8b,c). In this way the amplitude of the final arctangent function, evaluated subtracting the maximum value assumed by arctangent from the minimum (which in this case incidentally correspond to the initial and final value of the fit), provides our best estimation of the uplift of the sea floor at the CUMAS station. The value for the uplift during the 2011 episode is 2.5 cm (Figure 8b, blue line).

To test the stability of our procedure we iterate recursively between the last two operations and check the invariance of the residual time series (Figure 8d). Mathematically this procedure consists of successive application of a series of operators to the raw data: in our case we firstly perform tide removal, then we correct the bottom pressure data for water density variations and finally we subtract the modeled contribution of the vertical deformation and of the instrumental drift.

It must be emphasized that in general the composition of operators does not commute, i.e.:

$$f \circ g \neq g \circ f$$

The right order of operator composition is determined by the amplitude of the effect to be removed, from the greater amplitude to the smaller one.

We remove the seafloor uplift (represented by the fitting arctangent function) and the instrumental drift of the BPR sensor from the residual time series of Figure 8a to obtain the environmental and the instrumental noise represented by the terms E(t) and O(t) of equation (4) (Figure 9). It is worth noting that the mean value of the residual time series shown in figure 9 is about 0 and the residual data are well distributed around 0. The variance of this temporal series (about 1.27 cm) provides an estimation of the uncertainty on the measurement of the vertical deformation at the sea floor obtained by our analysis of the BPR data.

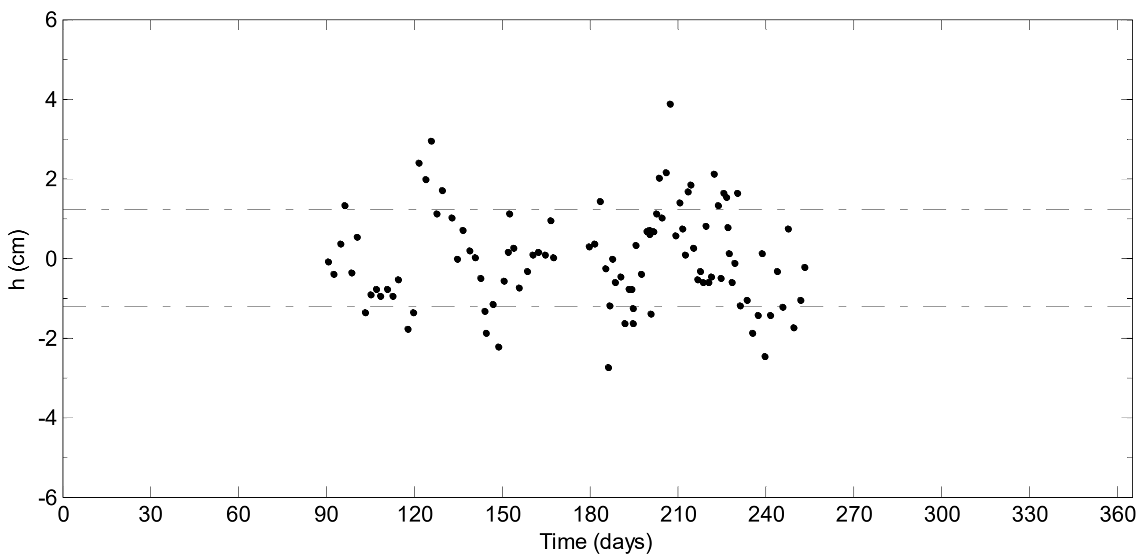

Figure 9. Environmental noise from the pressure signal.

As expected from the location of CUMAS BPR and the previous modeling of the source of deformation, the estimated vertical deformation at CUMAS site has a value in-between that of the observed uplift at POZZ and MISE (Figure 10).

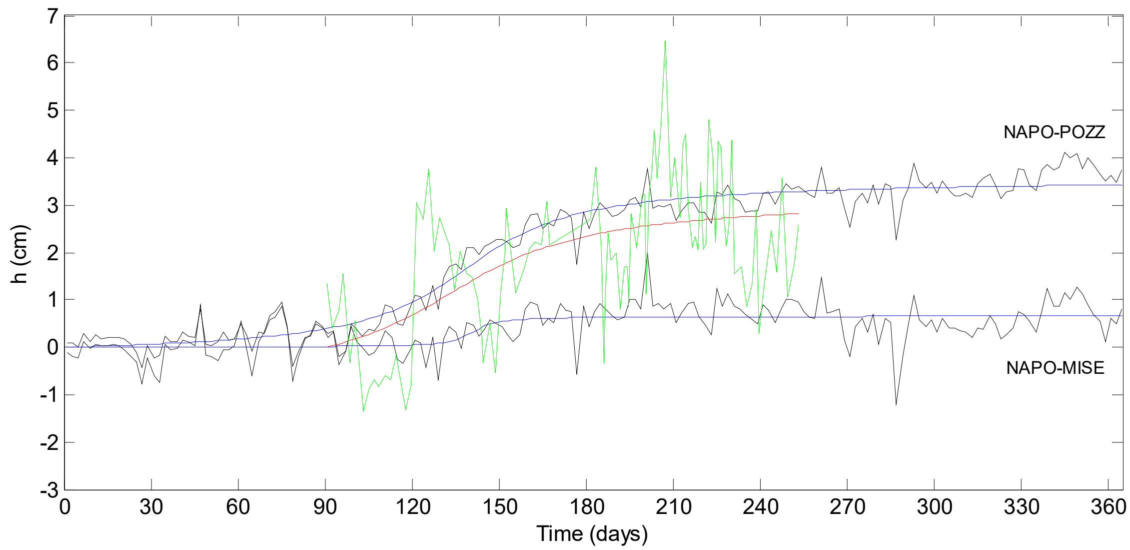

Figure 10. Estimation of vertical deformation observed at POZZ, MISE (black lines) with the respective best fitted inverse tangent (blue lines) compared with the estimated deformation at the CUMAS-BPR site (green line) and relative best fit arctangent (red line). As expected the value of the vertical deformation at the CUMAS site falls between the POZZ and MISE values.

In the particular case of long-term linear seafloor deformation and instrumental drifts with very similar trends (i.e. straight lines with the same angular coefficients), the application of a recursive best fit must be carefully considered. In fact in this case it can lead to an estimation of the deformation remarkably deviating from the true value with time.

5 Discussion and Conclusions

In this paper we demonstrate how by integrating observations at tide gauges, environmental measurements of salinity, temperature and atmospheric pressure, and bottom pressure data, it is possible to improve the resolution of sea-bottom measurements acquired by BPRs to estimate seafloor displacement on the order of a few centimeters in shallow water environment. The technical features of present day quartz based BPRs make them an ideal tool to assess very small hydrostatic pressure variations which can be converted into seafloor vertical displacements. However, the drift suffered by these sensors, along with seawater density changes and other pressure fluctuations produced by other sources, have similar magnitude and temporal scales to the volcanic deformation we want to measure. These other sources must be carefully evaluated and removed to reach a measurement resolution of about one centimeter in the estimation of vertical displacement. As described in the previous sections, and already suggested by Gennerich and Villinger [2011], to accomplish this goal auxiliary measurements are needed.

Here we used local atmospheric pressure measurements, CTD profiles, and tide gauge data to separate the contribution of BPR instrumental drift from the variation of pressure due to vertical sea floor movement. The drift shows an initial exponential decay during the first 15 days after the start of data acquisition (less than 10% of the full time of data collection, (Figure 8c) and a flat linear trend thereafter. The overall effect on the measurement (Figures 4 and 8) is about 1 cm of equivalent water height. It is possible that the low drift observed is also related to the fact that we are operating in shallow water [Wearn and Larson, 1982]. To minimize the effect of instrumental drift in the first few weeks after deployment, we start the data acquisition more than 1 month after the BPR deployment. The correction of the BPR time series for drift allows us to estimate the vertical seafloor displacement.

The method we have developed relies on a guess of the deformation character, which in the present case is retrieved from tide gauge measurements. However this important information can be recovered also from other measurements, as for instance from GPS time series, or from the method itself. The procedure outlined in figure 5, provide a recipe to find out the character of the deformation, by trying different functional forms and choosing the one which minimize the rms of the residual and the number of free parameters, in particular if non drifting or self calibrating bottom pressure recorder can be used ([Gennerich and Villinger, 2015]; [Sasagawa and Zumberge, 2013]).

Between 2011 and 2013, the Campi Flegrei volcanic area experienced an unrest phase with a cumulative uplift of about 16 cm measured by the GPS station RITE within the Pozzuoli town [DeMartino et al., 2014b]. Trasatti et al. [2015] used a data set of COSMO-SkyMed SAR and GPS observations and modeled a moment tensor point source in a 3-D heterogeneous material. Their results suggest that the caldera inflation can be explained by the emplacement of magma in a sill shaped body at a depth of about 5 km. The model locates the magma source near the coastline close to Pozzuoli. Figure 11a shows the pattern of the vertical displacement for the period 2011-2013 using the model of Trasatti et al [2015]. The green triangle on Figure 11 shows the location of the BPR used in this study and the green square represents the GPS station STRZ [DeMartino et al, 2014b]. According to the Trasatti et al. [2015] model these two locations should have experienced a similar amount of deformation. Indeed, the two datasets are compatible and show significant agreement well within the experimental uncertainties.

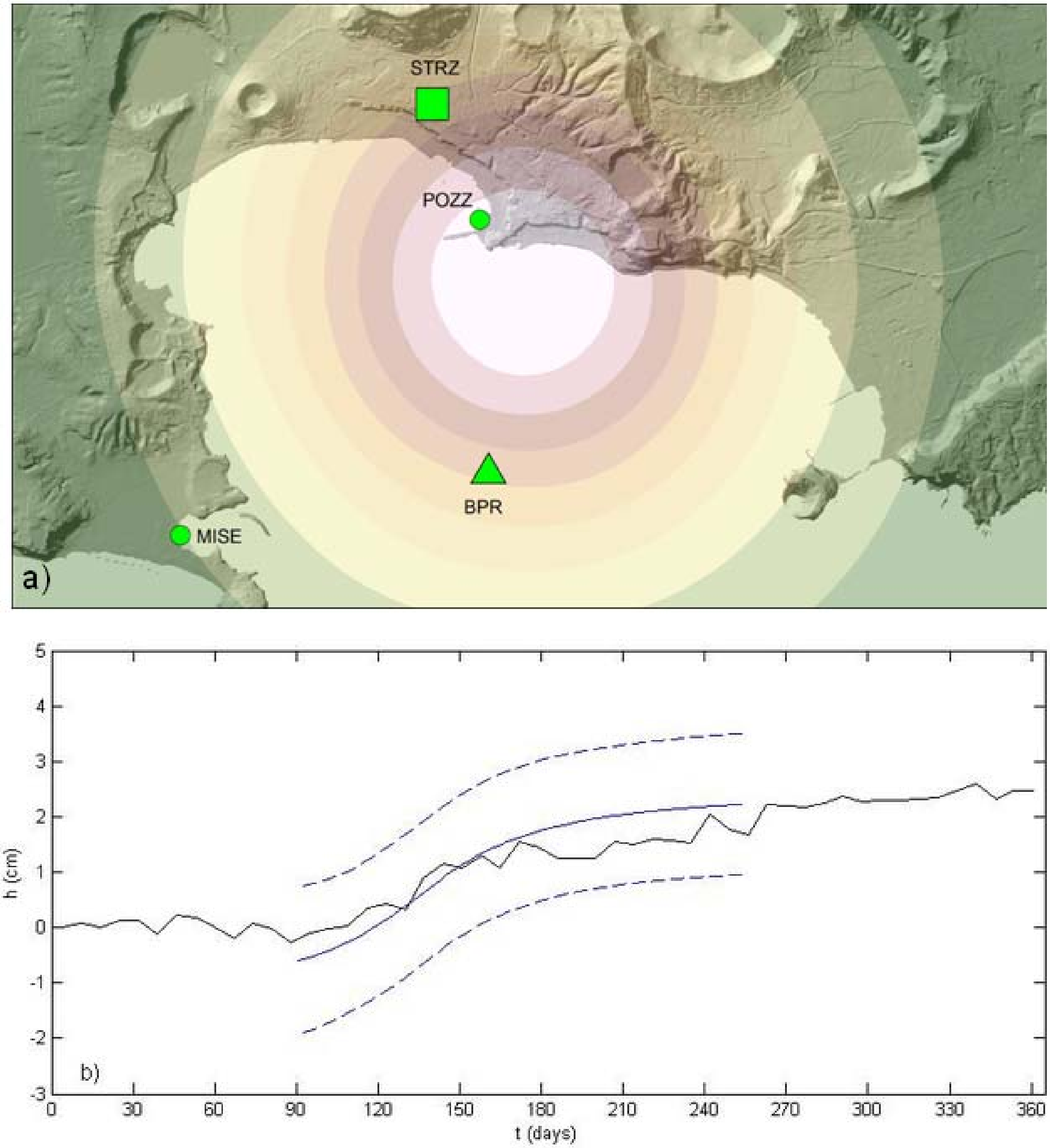

Figure 11. a) Vertical displacement pattern expected by the Trasatti at al. [2015] source model. The pattern is superimposed on the shaded relief map of the Campi Flegrei volcanic area. The

green triangle shows the position of the CUMAS system and the BPR. The green square shows the position of the CGPS station STRZ which recorded about 2.2 cm of uplift during the 6 months of BPR operation. The green circles show the position of Pozzuoli (POZZ) and Capo Miseno (MISE) tide gauges. The BPR and the STRZ-CGPS sites are located in areas that according to the model of Trasatti et al. [2015] should have experienced similar deformation history; **b**) Comparison between estimated vertical seafloor deformation at CUMAS site with relative 95% confidence interval (blue lines) and the vertical deformation observed at STRZ CGPS site (black line). The two curves show excellent agreement well within the calculated uncertainties.

Although the BPR data suffers from greater uncertainties than the GPS the estimated deformation in terms of trend and amplitude shows significant agreement with the observations at the GPS site STRZ.

This measurement of 2.5 +/-1.3 cm of vertical seafloor deformation represents the first measurement performed by a BPR in this high-risk volcanic area, demonstrating the potential for this technology as a monitoring tool, even in shallow water. Expanding our ability to estimate seafloor displacement could significantly improve the constraints available for deformation models of submerged caldera processes as well as monitoring other processes that produce shallow water deformation. The integration of BPR sensors with existing land-based networks allows for the expansion of geodetic monitoring into coastal waters and shallow marine environments. INGV has also been experimenting with the use of a GPS sensor on the buoy of the CUMAS system [De Martino et al., 2014a] which showed about 4 cm of uplift during 2012-2013 [De Martino et al., 2014a]. These are two new geodetic methodologies to monitor volcanic areas, or zones of local deformation, in coastal waters. The installation of 3 more systems combining BPR and GPS sensors is currently underway in the Gulf of Pozzuoli to expand this monitoring effort.

Acknowledgments and Data

We thank Stazione Zoologica Anton Dohrn of Naples for providing the CTD profiles used in this study.

(http://szn.macisteweb.com/front-page-en-en-en?set_language=en).

Atmospheric pressure time series are available at the Rete Mareografica Nazionale website operated by ISPRA (http://www.mareografico.it).

We also thank Elisa Trasatti who kindly provided the dataset used to produce the map of the Campi Flegrei 2011-2013 deformation model.

We thank Professor William Chadwick for the very useful suggestions, comments and corrections which improved the original manuscript. We also thank the anonymous referee.

BPR and tide gauges data are available upon request to G. Iannaccone (giovanni.iannaccone@ingv.it).

References

Amoruso, A., L. Crescentini, and I. Sabbetta (2014a), Paired deformation sources of the Campi Flegrei caldera (Italy) required by recent (1980–2010) deformation history, J. Geophys. Res. Solid Earth, 119, 858–879, doi:10.1002/2013JB010392.

Amoruso, A., L. Crescentini, I. Sabbetta, P. De Martino, F. Obrizzo, and U. Tammaro (2014b), Clues to the cause of the 2011–2013 Campi Flegrei caldera unrest, Italy, from continuous GPS data, Geophys. Res. Lett., 41, 3081–3088

Ballu, V., Ammann, J., Pot, O., De Viron, O., Sasagawa, G. S., Reverdin, G., Bouin M., Cannat M., Deplus C., Deroussi S., Maia M., Diament M. (2009). A seafloor experiment to monitor vertical deformation at the Lucky Strike volcano, Mid-Atlantic Ridge. Journal of Geodesy, 83(2), 147-159.

Bernard, E., and C. Meinig (2011). History and future of deep-ocean tsunami measurements. In Proceedings of Oceans' 11 MTS/IEEE, Kona, IEEE, Piscataway, NJ, 19–22 September 2011, No. 6106894, 7 pp.

Berrino, G. (1998). Detection of vertical ground movements by sea-level changes in the Neapolitan volcanoes. Tectonophysics, 294(3), 323-332.

Burgmann, R, Chadwell D. (2014). Seafloor geodesy. Annual Review of Earth and Planetary Sciences, Vol 42. 42:509-534.

Caloi, P., & Marcelli, L. (1949). Oscillazioni libere del Golfo di Napoli. Annals of Geophysics, 2(2), 222-242.

Chadwick, W. W., Nooner, S. L., Zumberge, M. A., Embley, R. W., & Fox, C. G. (2006). Vertical deformation monitoring at Axial Seamount since its 1998 eruption using deep-sea pressure sensors. Journal of Volcanology and Geothermal Research, 150(1), 313-327.

Chadwick Jr, W. W., Nooner, S. L., Butterfield, D. A., & Lilley, M. D. (2012). Seafloor deformation and forecasts of the April 2011 eruption at Axial Seamount. Nature Geoscience, 5(7), 474-477.

Corrado, G., Luongo, G. (1981). Ground deformation measurements in active volcanic areas using tide gauges. Bulletin Volcanologique, 44(3), 505-511.

D'Auria, L. et al. (2015) Magma injection beneath the urban area of Naples: a new mechanism for the 2012–2013 volcanic unrest at Campi Flegrei caldera. Sci. Rep. 5, 13100; doi:10.1038/srep13100.

Del Gaudio, C., Aquino, I., Ricciardi, G. P., Ricco, C., & Scandone, R. (2010). Unrest episodes at Campi Flegrei: A reconstruction of vertical ground movements during 1905–2009. Journal of Volcanology and Geothermal Research, 195(1), 48-56.

De Martino P., Guardato S., Tammaro U., Vassallo M., Iannaccone G. (2014a) A first GPS measurement of vertical seafloor displacement in the Campi Flegrei Caldera (Italy). Journal of Volcanology and Geothermal Research, vol. 276 pp. 145-151

De Martino, P., Tammaro, U., & Obrizzo, F. (2014b). GPS time series at Campi Flegrei caldera (2000-2013). Annals of Geophysics, 57(2), S0213.

Di Vito, M., Lirer, L., Mastrolorenzo, G., & Rolandi, G. (1987). The 1538 Monte Nuovo eruption (Campi Flegrei, Italy). Bulletin of Volcanology, 49, 608-615.

Di Vito, M. A., Isaia, R., Orsi, G., Southon, J., De Vita, S., d'Antonio, M., ... & Piochi, M. (1999). Volcanism and deformation since 12,000 years at the Campi Flegrei caldera (Italy). Journal of Volcanology and Geothermal Research, 91(2), 221-246.

Dziak, R. P., Haxel, J. H., Bohnenstiehl, D. R., Chadwick Jr, W. W., Nooner, S. L., Fowler, Matsumoto M. J., Butterfield, D. A. (2012). Seismic precursors and magma ascent before the April 2011 eruption at Axial Seamount. Nature Geoscience, 5(7), 478-482.

Dvorka, J.J., and D. Dzursin (1997). Volcano geodesy: The search for magma reservoirs and the formation of eruptive vents. Rev. Geophys. 35, 343-384. DOI: 10.1029/97RG00070.

Dzurisin D. (2006) Volcano Deformation: New Geodetic Monitoring Techniques. Springer Berlin Heidelberg, pag442,ISBN 9783540493020

Eble, M. C., & Gonzalez, F. I. (1991). Deep-ocean bottom pressure measurements in the northeast Pacific. Journal of Atmospheric and Oceanic Technology, 8(2), 221-233.

Fofonoff, P. and Millard, R.C. (1983) Algorithms for computation of fundamental properties of seawater. UNESCO Tech. Pap. in Mar. Sci., No. 44, 53 pp.

Fox, C. G. (1990), Evidence of active ground deformation on the mid-ocean ridge: Axial Seamount, Juan de Fuca Ridge, April-June, 1988, J. Geophys. Res., 95, 12813-12822

Fox, C. G. (1993), Five years of ground deformation monitoring on Axial Seamount using a bottom pressure recorder, Geophys. Res. Lett., 20(17), 1859-1862

Fox, C. G. (1999), In situ ground deformation measurements from the summit of Axial Volcano during the 1998 volcanic episode, Geophys. Res. Lett., 26(23), 3437-3440

Fox, C. G., W. W. Chadwick, Jr., and R. W. Embley (2001), Direct observation of a submarine volcanic eruption from a sea-floor instrument caught in a lava flow, Nature, 412, 727-729

Freymueller, J. T., J. B. Murray, H. Rymer, C. A. Locke (2015). Chapter 64 - Ground Deformation, Gravity, and Magnetics, In The Encyclopedia of Volcanoes (Second Edition), edited by Haraldur Sigurdsson, Academic Press, Amsterdam, 1101-1123, ISBN 9780123859389.

Gennerich, H.-H., and H. Villinger (2011), Deciphering the ocean bottom pressure variation in the Logatchev hydrothermal field at the eastern flank of the Mid-Atlantic Ridge, Geochemistry, Geophysics, Geosystems, 12, Q0AE03

Gennerich, H.-H., and H. Villinger (2015), A new concept for an ocean bottom pressure meter capable of precision long-term monitoring in marine geodesy and oceanography, Earth and Space Science, 2, 181–186, doi:10.1002/2014EA000053.

Hino, R., Inazu, D., Ohta, Y., Ito, Y., Suzuki, S., Iinuma, T., ... & Kaneda, Y. (2014). Was the 2011 Tohoku-Oki earthquake preceded by aseismic preslip? Examination of seafloor vertical deformation data near the epicenter. Marine Geophysical Research, 35(3), 181-190.

Houghton B.F. and I.A. Nairn (1991) The 1976–1982 strombolian and phreatomagmatic eruptions of White Island, New Zealand: eruptive and depositional mechanisms at a 'wet' volcano. Bull. Volcanol., 54 (1991), pp. 25–49

Iannaccone G., Guardato S., Vassallo M., Elia L., Beranzoli L., (2009) A new multidisciplinary marine monitoring system for the surveillance of volcanic and seismic areas, Seismological Research Letters, 80, 203-213

Iannaccone G., Vassallo M., Elia L., Guardato S., Stabile T.A., Satriano C., Beranzoli L. (2010) Long-term seafloor experiment with the CUMAS module: performance, noise analysis of geophysical signals, and suggestions about the design of a permanent network, Seismological Research Letters, 81, 916-927

Ikuta, R., K. Tadokoro, M. Ando, T. Okuda, S. Sugimoto, K. Takatani, K. Yada, and G. M. Besana (2008), A new GPS acoustic method for measuring ocean floor crustal deformation: Application to the Nankai Trough, J. Geophys. Res., 113, B02401

McGuire, J. J., & Collins, J. A. (2013). Millimeter-level precision in a seafloor geodesy experiment at the Discovery transform fault, East Pacific Rise. Geochemistry, Geophysics, Geosystems, 14(10), 4392-4402.
Mori, J., McKee, C., Itikarai, L., de Saint Ours, P., Talai B. (1986) Sea level measurements for inferring ground deformations in Rabaul Caldera. Geo-Marine Letters, Volume 6, Issue 4, 241-246

Nooner, S. L., & W. W. Chadwick, Jr. (2009). Volcanic inflation measured in the caldera of Axial Seamount: Implications for magma supply and future eruptions, Geochemistry, Geophysics, Geosystems, 10, Q02002, doi:10.1029/2008GC002315.

Paradissis, D., Drakatos, G., Marinou, A., Anastasiou, D., Alatza, S., Zacharis, V., ... & Makropoulos, K. (2015). South Aegean Geodynamic And Tsunami Monitoring Platform. In EGU General Assembly Conference Abstracts (Vol. 17, p. 6270).

Pawlowicz, R., Beardsley, B., & Lentz, S. (2002). Classical tidal harmonic analysis including error estimates in MATLAB using T_TIDE. Computers & Geosciences, 28(8), 929-937.

Phillips, K. A., C. D. Chadwell, and J. A. Hildebrand (2008), Vertical deformation measurements on the submerged south flank of Kilauea volcano, Hawaii reveal seafloor motion associated with volcanic collapse, J. Geophys. Res., 113, B05106, doi:10.1029/2007JB005124.

Polster, A., Fabian, M., & Villinger, H. (2009). Effective resolution and drift of Paroscientific pressure sensors derived from longterm seafloor measurements. Geochemistry, Geophysics, Geosystems, 10(8).

Pyle, D.M., 1998. Forecasting sizes and repose times of future extreme volcanic events. Geology 26, 367–370.

Sasagawa, G., & Zumberge, M. A. (2013). A self-calibrating pressure recorder for detecting seafloor height change. IEEE Journal of Oceanic Engineering, 38(3), 447-454.

Self, S., 1983. Large-scale phreatomagmatic silicic volcanism: A case study from New Zealand. J. Volcanol. Geotherm. Res. 17, 433–469.

Sparks, R.S.J., 2003. Forecasting volcanic eruptions. Earth Planet. Sci. Lett. 210, 1–15.

Speich, S., & Mosetti, F. (1988). On the eigenperiods in the Tyrrhenian Sea level oscillations. Il Nuovo Cimento C, 11(2), 219-228.

Spiess, F. N., C. D. Chadwell, J. A. Hildebrand, L. E. Young, G. H. Purcell Jr., and H. Dragert (1998). Precise GPS/acoustic positioning of seafloor reference points for tectonic studies, Phys. Earth Planet. Inter., 108, 101– 112.

Tammaro U., Obrizzo F., De Martino P., La Rocca A., Pinto S., Vertechi E., Capuano P. (2014) Spectral Characteristics of Sea Level Gauges for Ground Deformation Monitoring at Neapolitan Active Volcanoes: Somma-Vesuvius, Campi Flegrei caldera and Ischia island

Trasatti, E., M. Polcari, M. Bonafede, and S. Stramondo (2015), Geodetic constraints to the source mechanism of the 2011–2013 unrest at Campi Flegrei (Italy) caldera, Geophys. Res. Lett., 42, 3847–3854, doi:10.1002/2015GL063621.

Wallace, L. M., Webb, S. C., Ito, Y., Mochizuki, K., Hino, R., Henrys, S., ... & Sheehan, A. F. (2016). Slow slip near the trench at the Hikurangi subduction zone, New Zealand. Science, 352(6286), 701-704.

Ward, S.N., Day, S., 2001. Cumbre Vieja Volcano -- Potential collapse and tsunami at La Palma, Canary Islands. Geophys. Res. Lett. 28, 3397–3400.

Watts, D. R., & Kontoyiannis, H. (1990). Deep-ocean bottom pressure measurement: Drift removal and performance. Journal of Atmospheric and Oceanic Technology, 7(2), 296-306.

Wearn, R. B., & Larson, N. G. (1982). Measurements of the sensitivities and drift of Digiquartz pressure sensors. Deep Sea Research Part A. Oceanographic Research Papers, 29(1), 111-134.

Wunsch, C., & Stammer, D. (1997). Atmospheric loading and the oceanic “inverted barometer” effect. Reviews of Geophysics, 35(1), 79-107.

Figure 1.

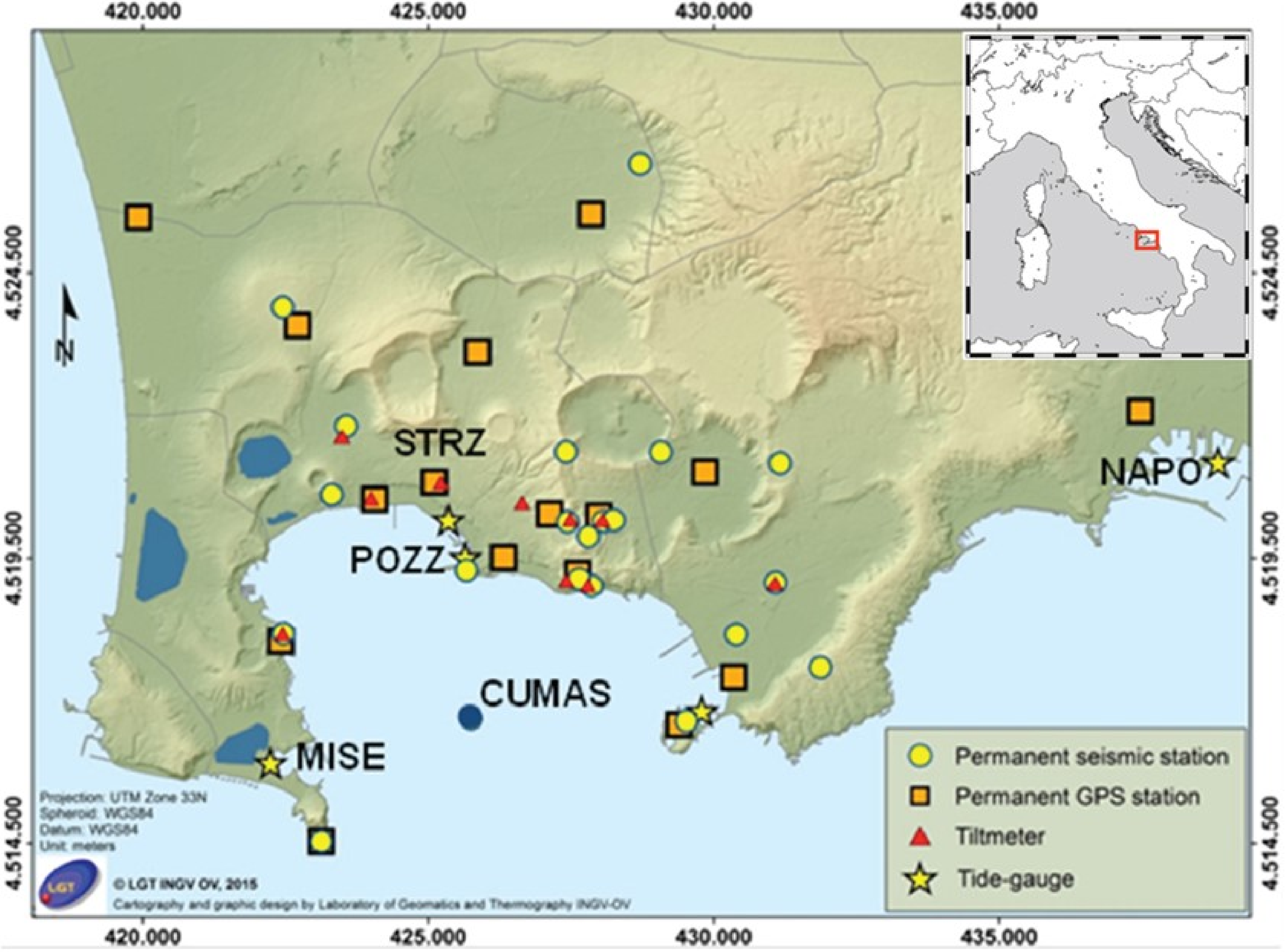

420.000
425.000
430.000
435.000
4.524.500
4.519.500
4.514.500
N
STRZ
POZZ
NAPO
CUMAS
MISE
Permanent seismic station
Permanent GPS station
Tiltmeter
Tide-gauge
Projection: UTM Zone 33N
Spheroid: WGS84
Datum: WGS84
Unit: meters
LGT
© LGT INGV OV, 2015
Cartography and graphic design by Laboratory of Geomatics and Thermography INGV-OV

Figure 2.

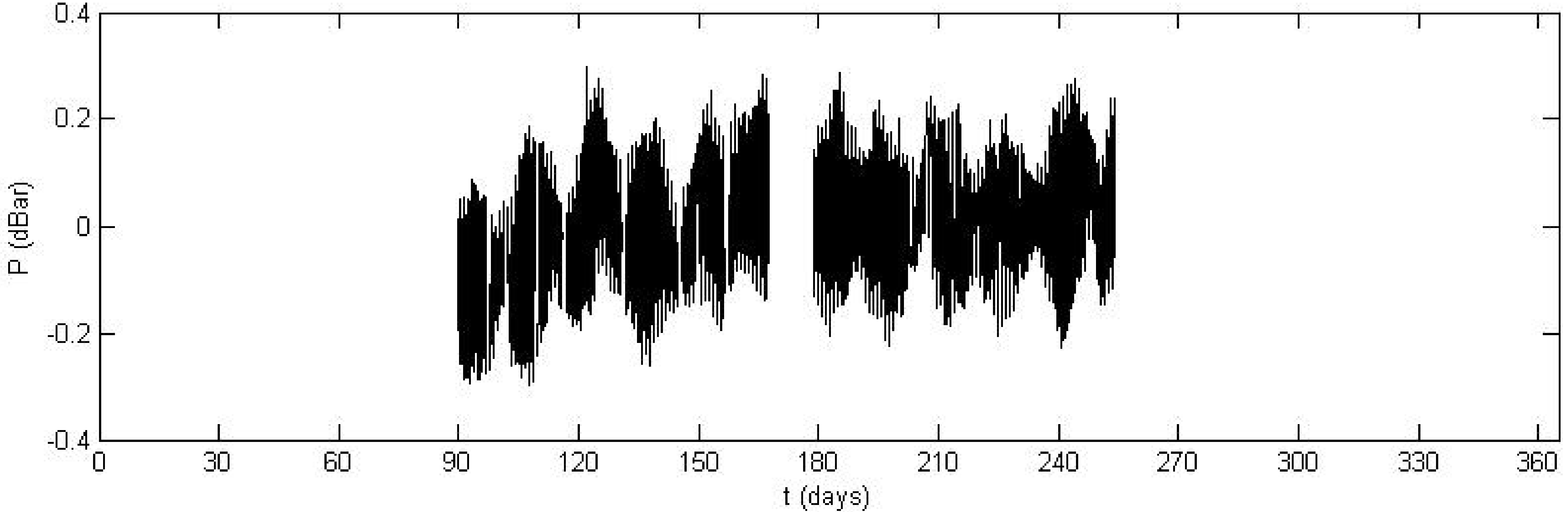
0.4
0.2
0
-0.2
-0.4
P (dBar)
0
30
60
90
120
150
180
210
240
270
300
330
360
t (days)

Figure 3.

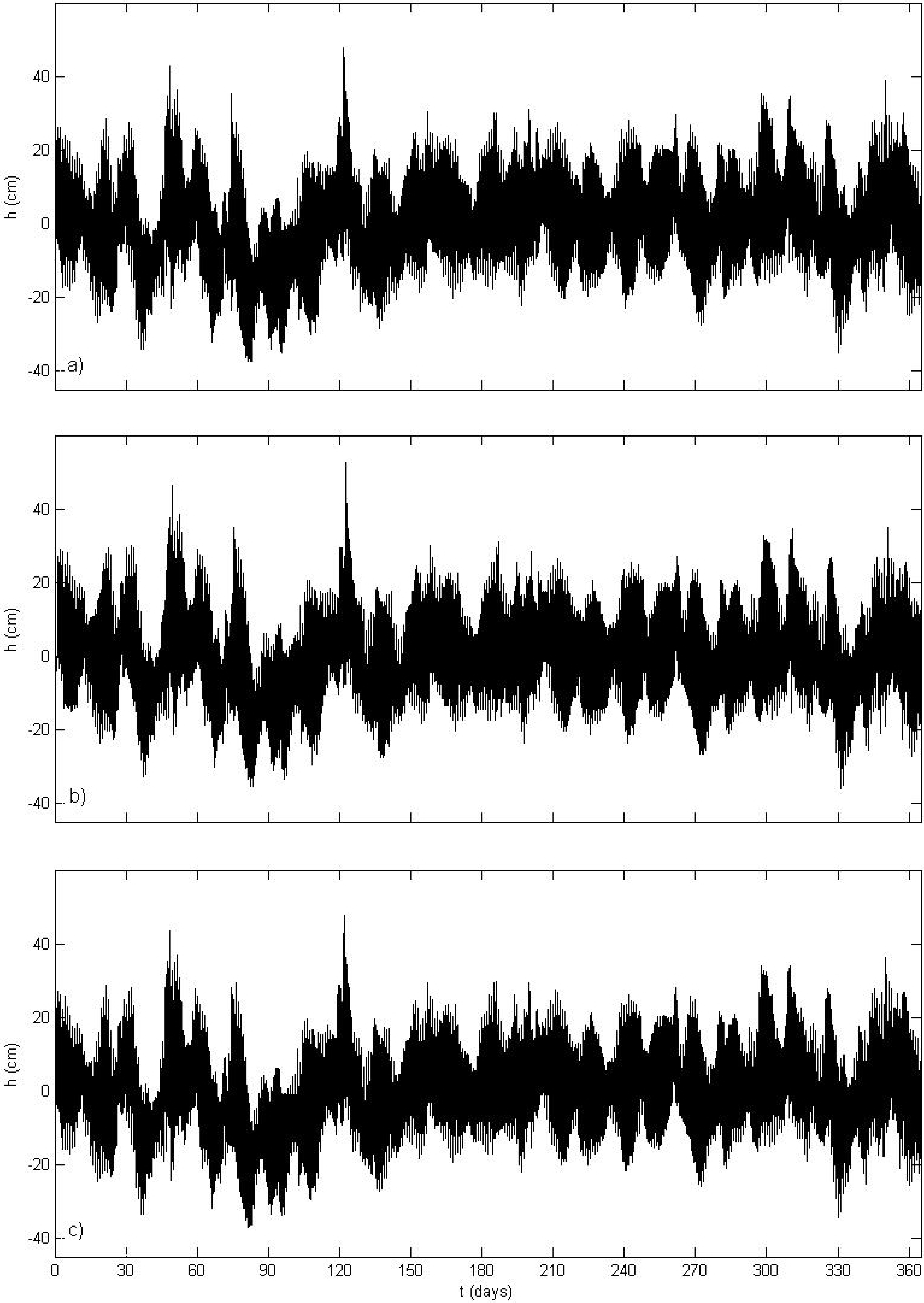

h (cm)
40
20
0
-20
-40
a)
b)
c)
0
30
60
90
120
150
180
210
240
270
300
330
360
t (days)

Figure 4.

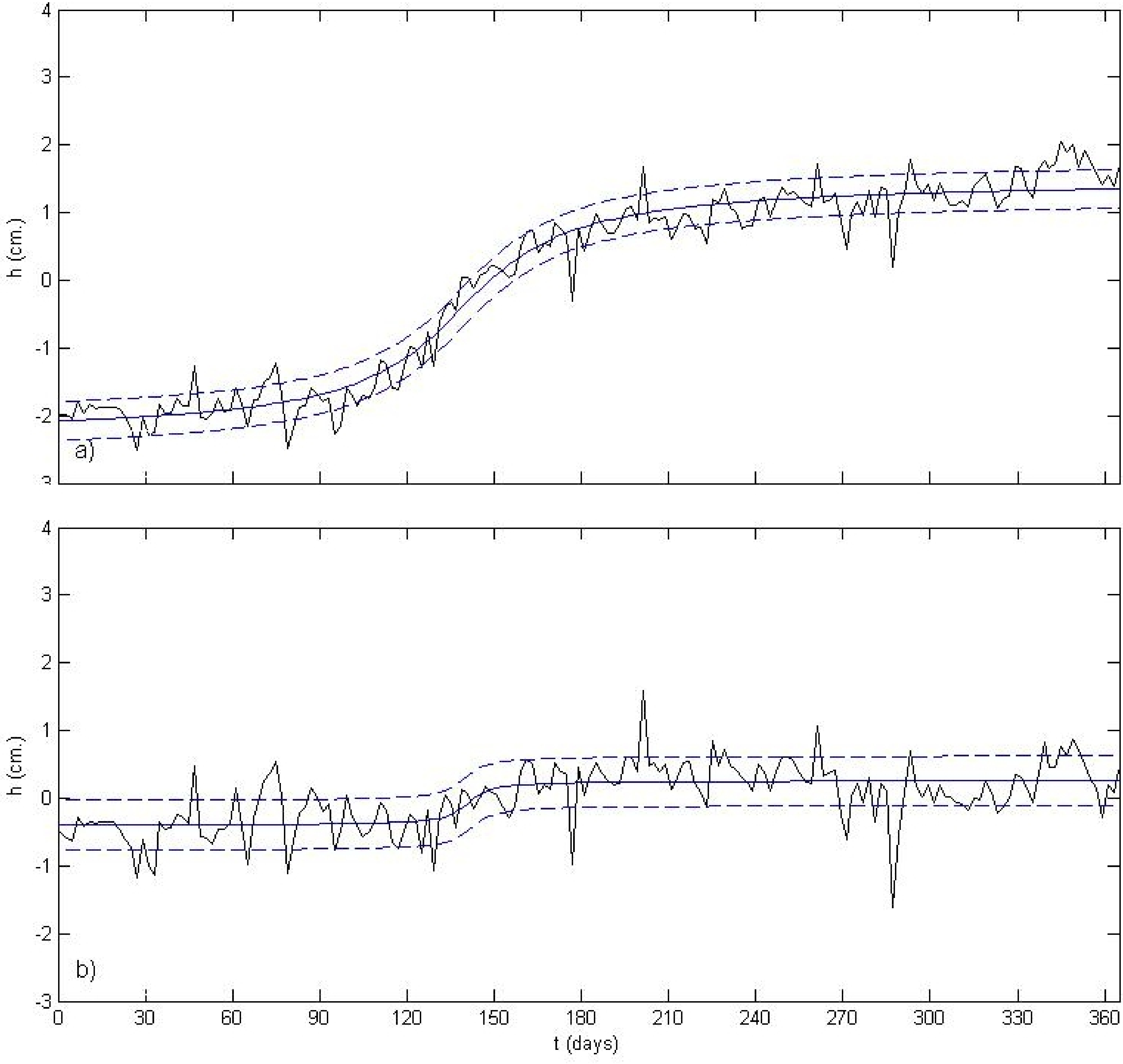

h (cm.)
a)
h (cm.)
b)
t (days)
0
30
60
90
120
150
180
210
240
270
300
330
360

Figure 5.

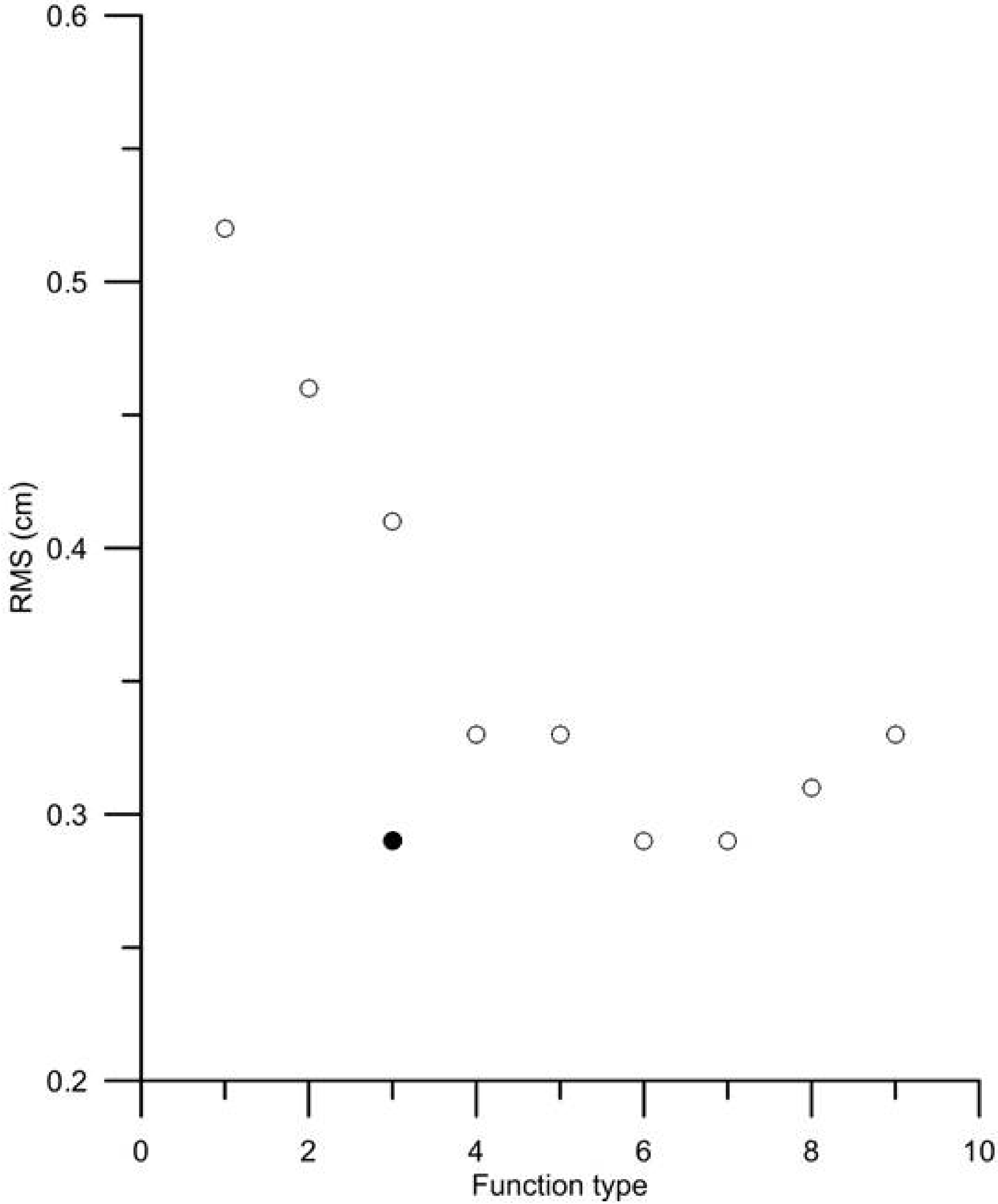

0.6
0.5
0.4
0.3
0.2
RMS (cm)
0
2
4
6
8
10
Function type

Figure 6.

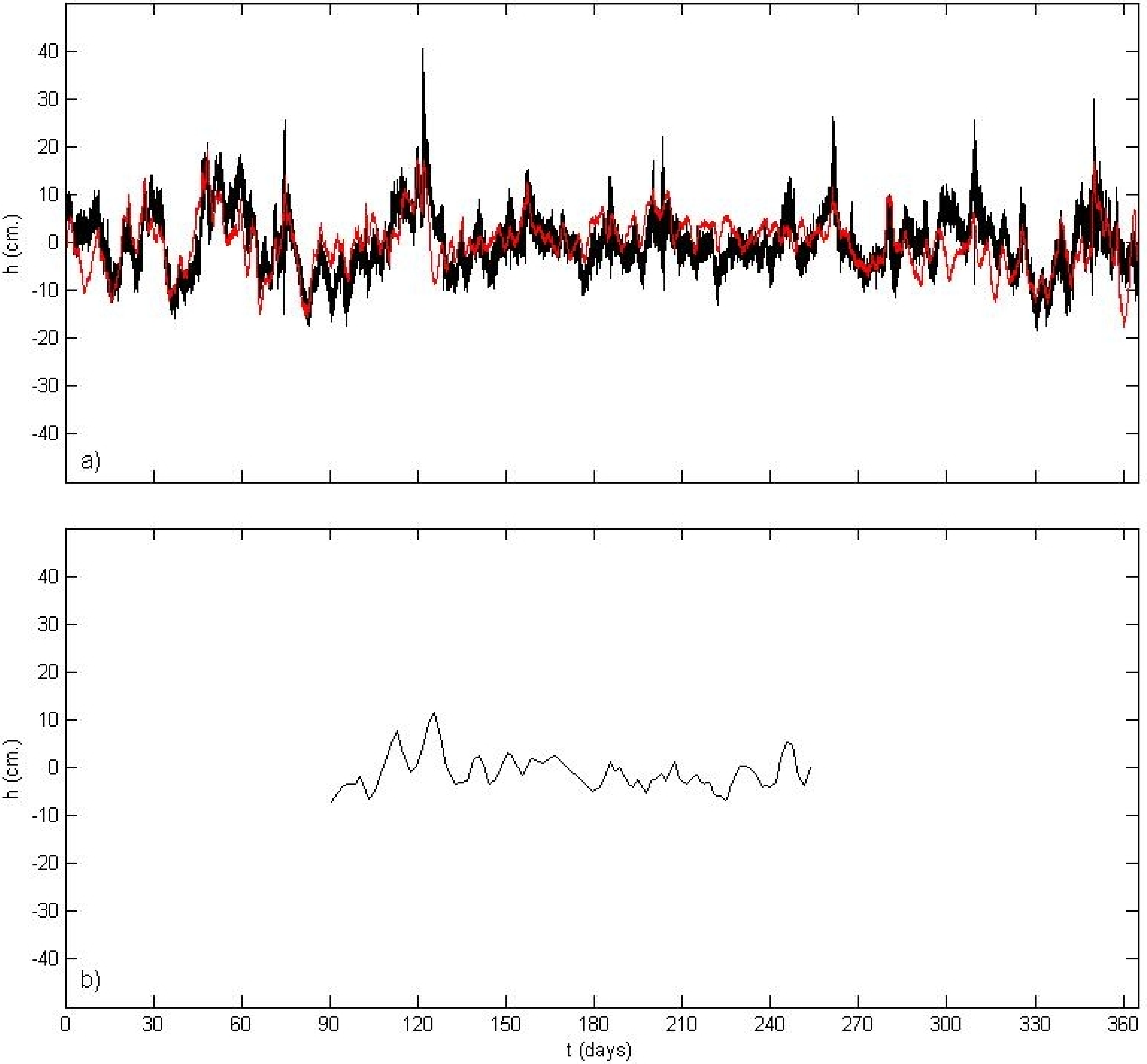

a)
h (cm.)
40
30
20
10
0
-10
-20
-30
-40
b)
h (cm.)
40
30
20
10
0
-10
-20
-30
-40
0
30
60
90
120
150
180
210
240
270
300
330
360
t (days)

Figure 7.

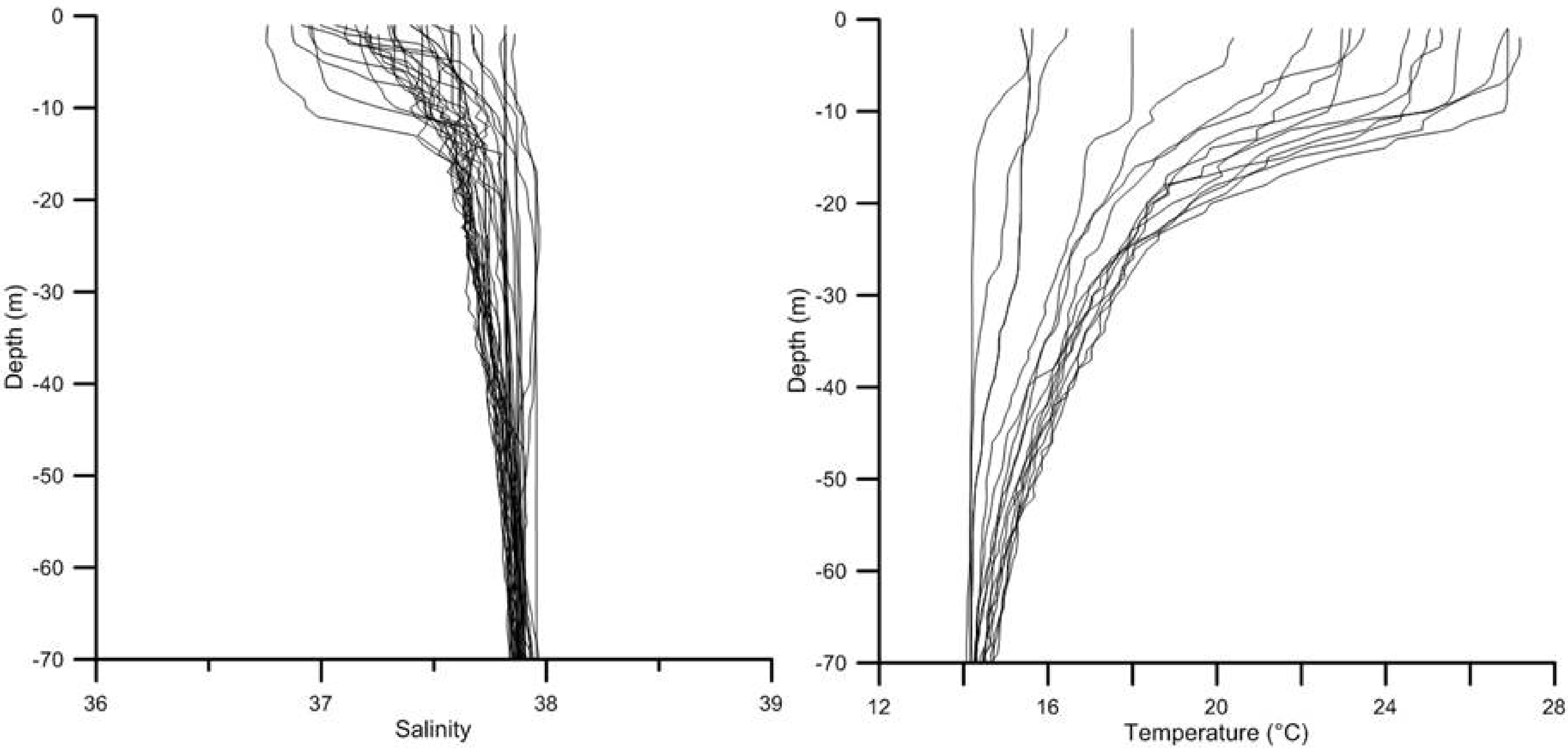

Depth (m)
0
-10
-20
-30
-40
-50
-60
-70
36
37
38
39
Salinity
Depth (m)
0
-10
-20
-30
-40
-50
-60
-70
12
16
20
24
28
Temperature (°C)

Figure 8.

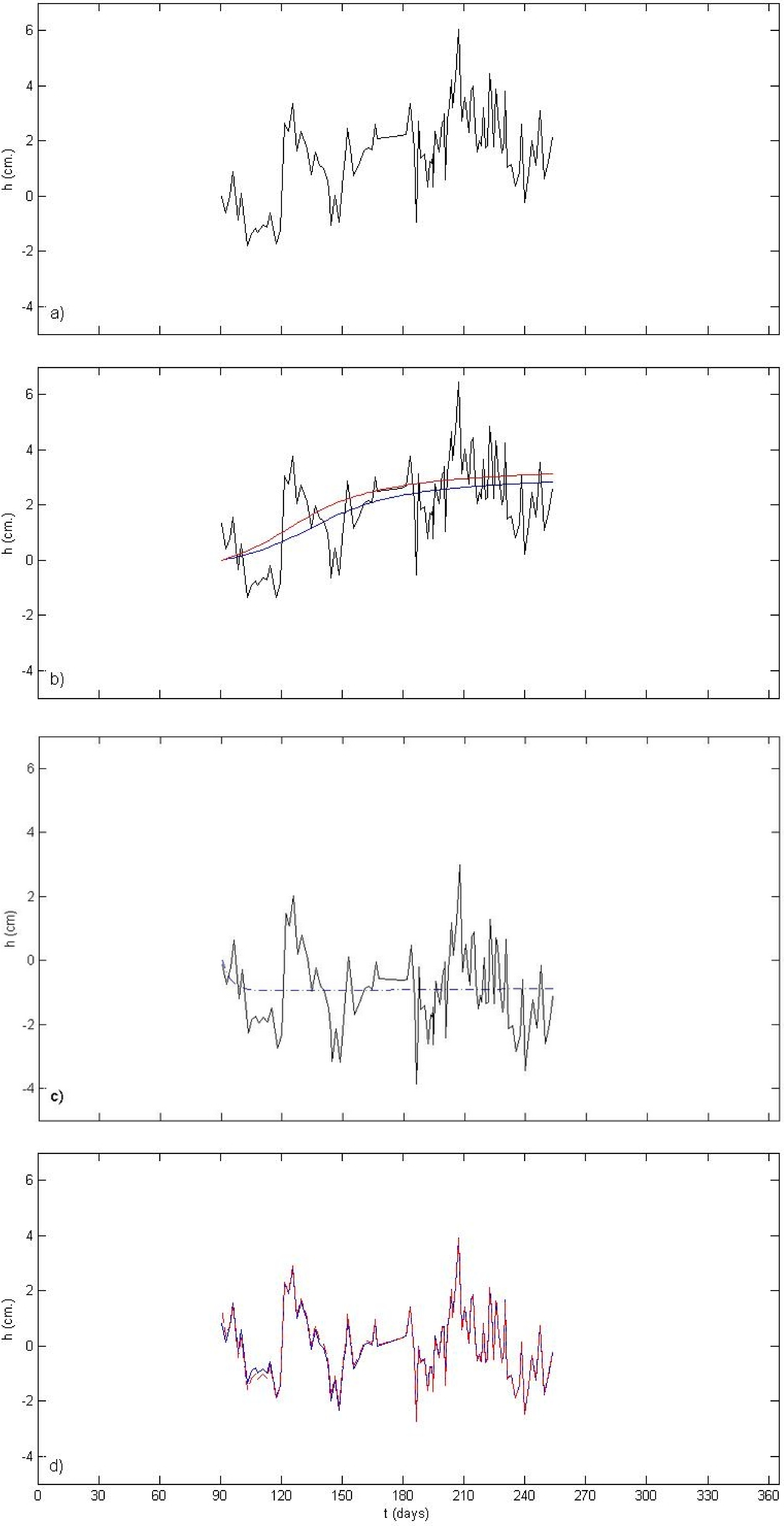

h (cm.)
a)
b)
h (cm)
c)
d)
t (days)

Figure 9.

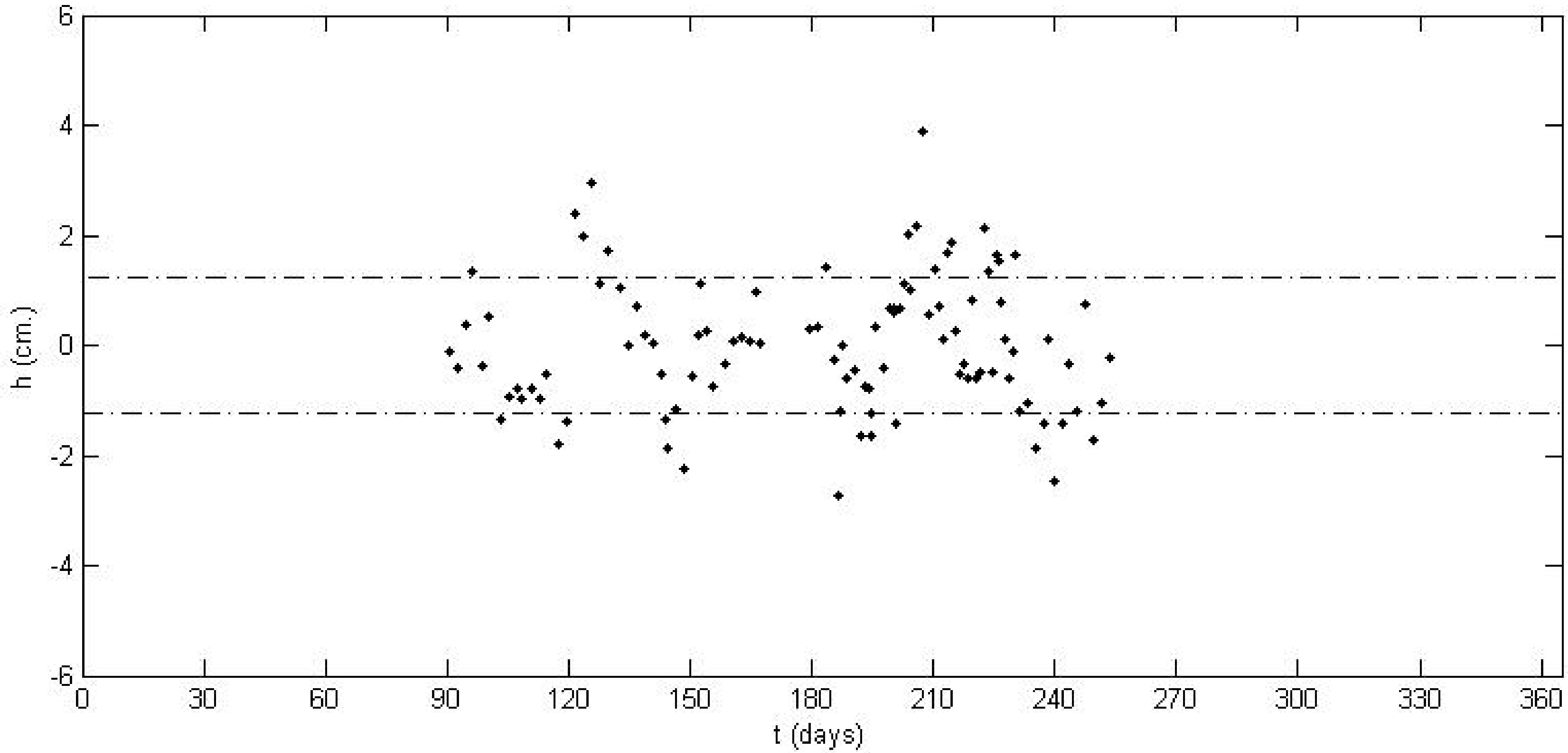
h (cm.)
t (days)
6
4
2
0
-2
-4
-6
0
30
60
90
120
150
180
210
240
270
300
330
360

Figure 10.

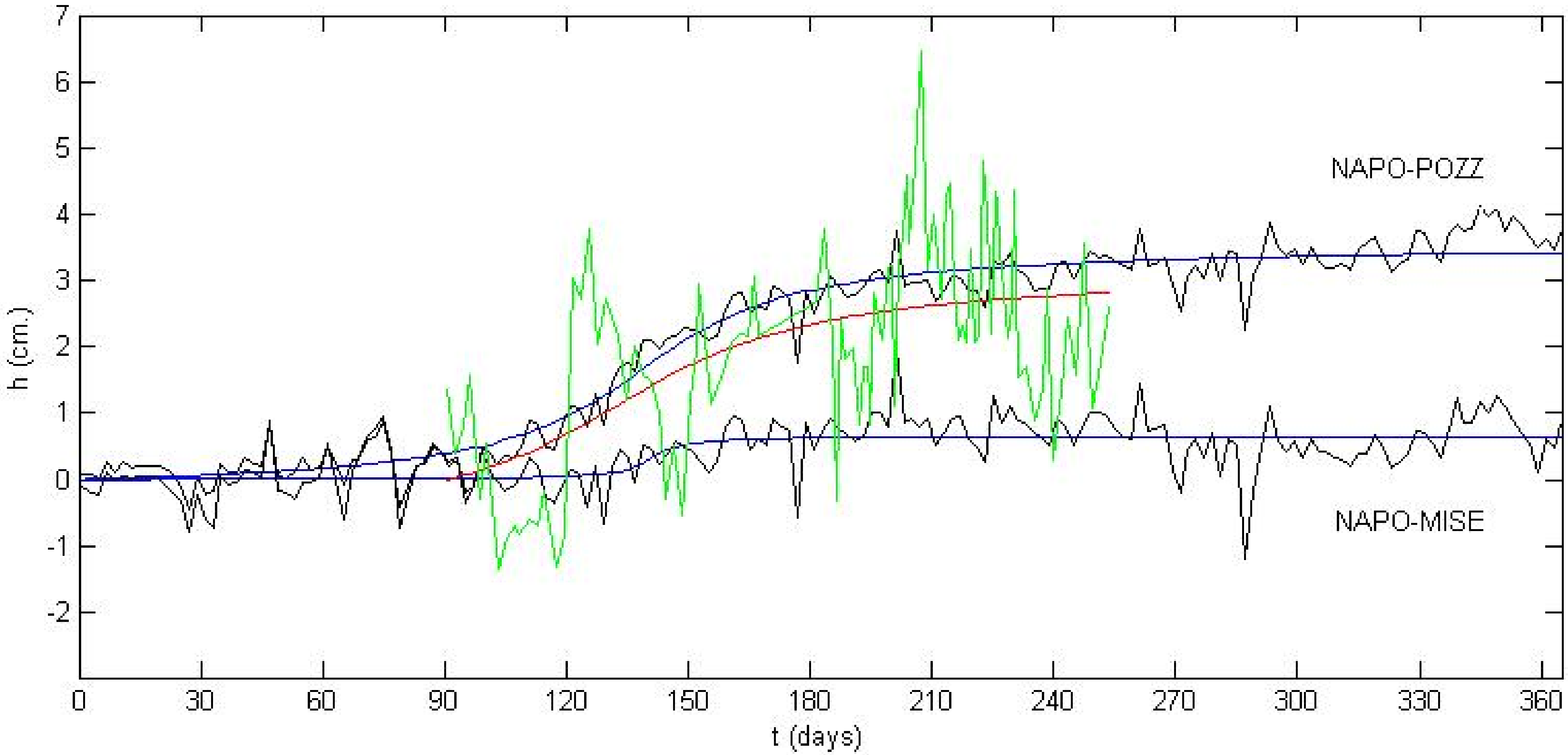

7
6
5
4
3
2
1
0
-1
-2
h (cm.)
NAPO-POZZ
NAPO-MISE
0
30
60
90
120
150
180
210
240
270
300
330
360
t (days)

Figure 11.

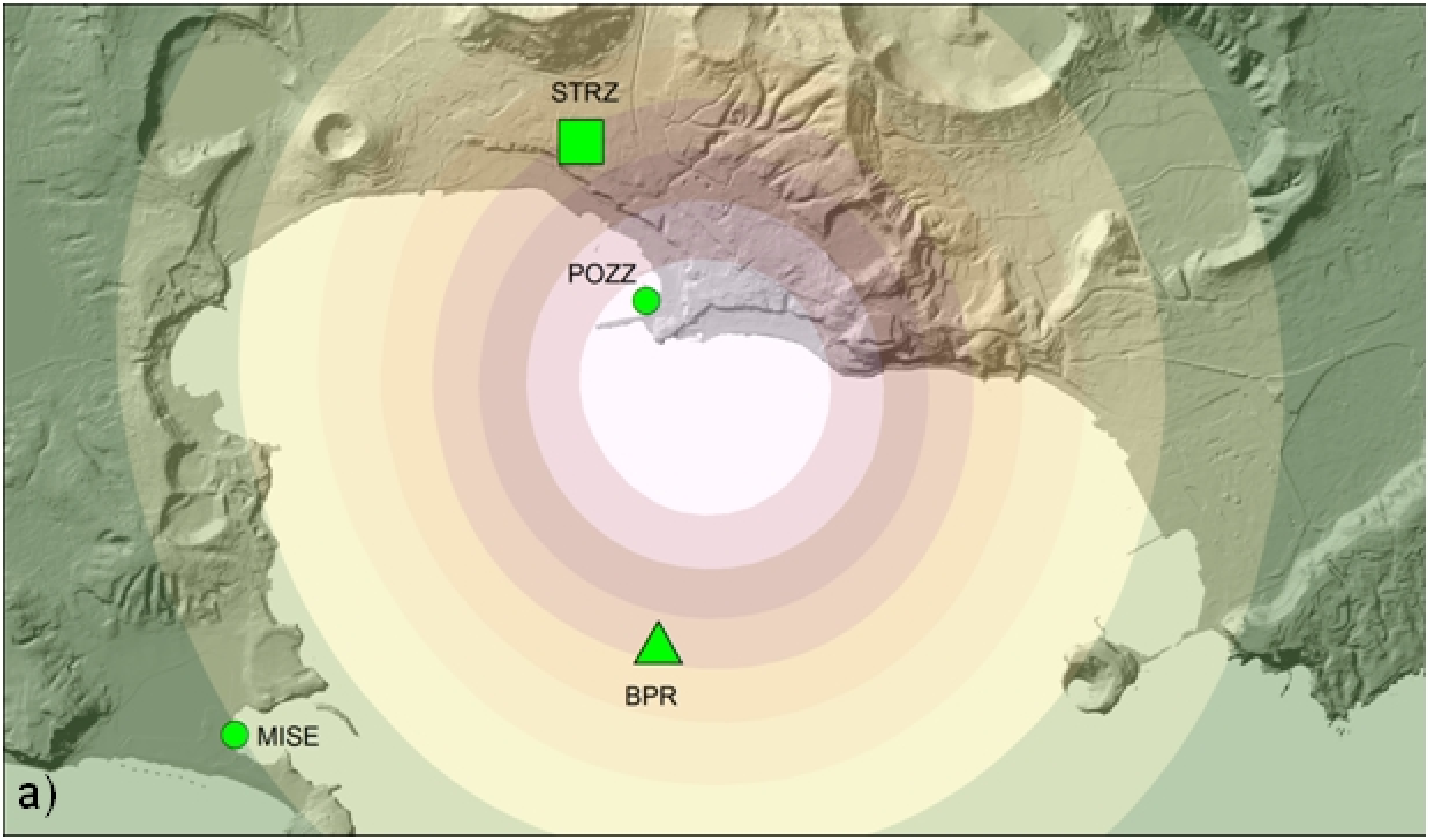
STRZ
POZZ
BPR
MISE
a)

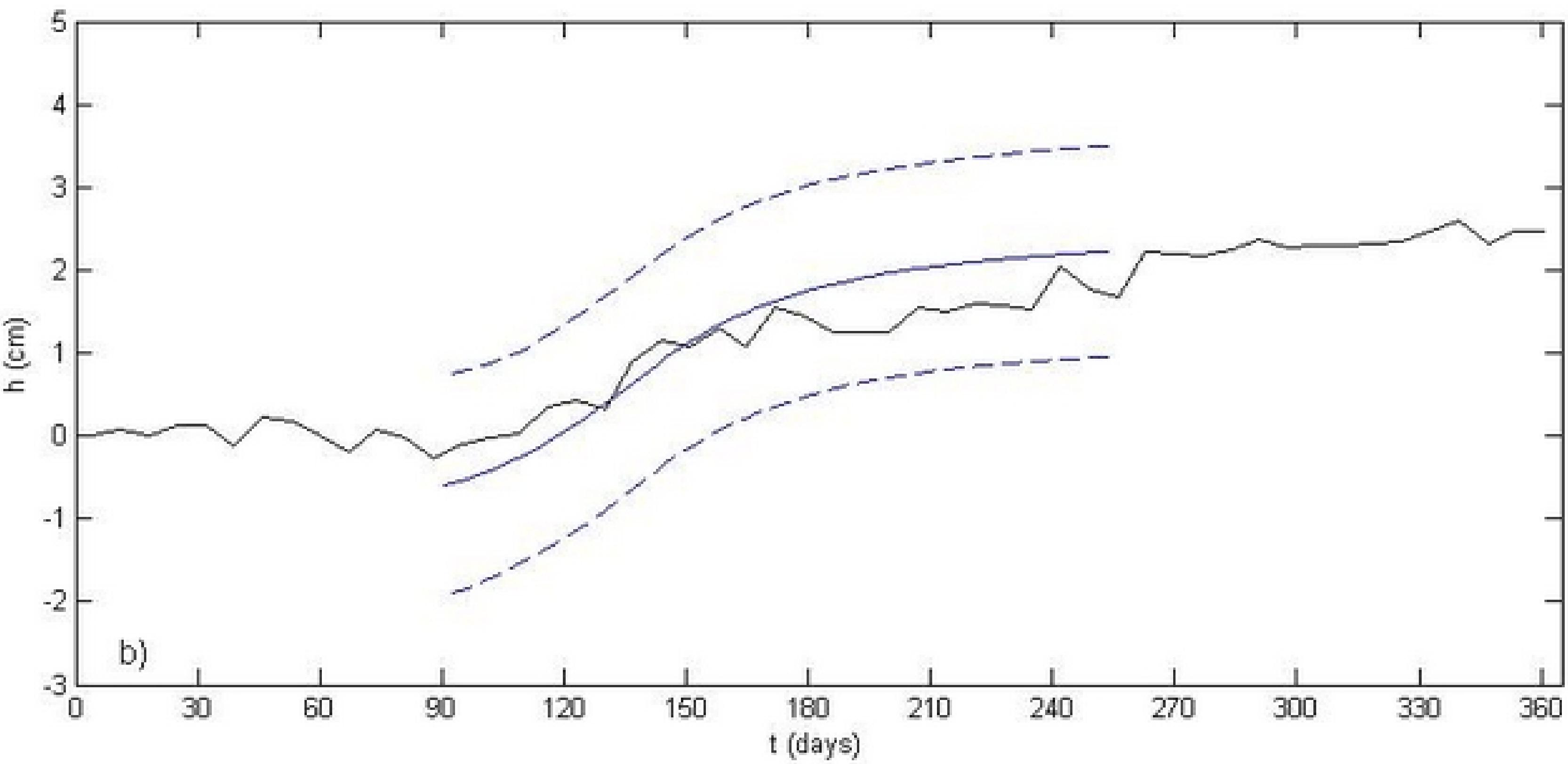
h (cm)
t (days)
b)
5
4
3
2
1
0
-1
-2
-3
0
30
60
90
120
150
180
210
240
270
300
330
360